Comparative Analysis of Simplified Biochemical Models for Thrombosis Simulation via the Viscosity Variation Method.

Georgios Kotsidis

Computational Mechanics MSc

School of Chemical Engineering

National Technical University of Athens

September 2023

A thesis submitted for the degree of
Master of Science

Supervisor: Asst. Prof. Mihalis Kavousanakis

Contents

List of Figures

List of Tables

Chapter 1

Introduction

This research aims to critically examine viscosity fluctuations as a potential method for simulating clotting scenarios. Initially, a comprehensive review of existing simulation methodologies will be undertaken. Following this, three streamlined biochemical depictions of clot formation will be presented. The commonalities, assumptions, and fluid mechanics tactics employed across these models will be highlighted.

Simulations will be conducted on two distinct geometries(2d and 3d), drawing from prior in vitro experiment, each possessing unique rheological attributes.

1.1 Background and Significance of Thrombosis Research

Thrombosis, a pervasive health concern, is characterized by the untimely formation of thrombi within blood vessels. Such formations can impede regular vascular flow, leading to notable clinical episodes like myocardial infarctions, strokes, and venous thromboembolisms. Its global impact is evident, with thrombosis-associated ailments recognized by the World Health Organization as major contributors to morbidity and mortality.

Delving into the intricacies of thrombosis is of paramount importance. Its genesis can be attributed to a combination of cellular dynamics, biochemical cascades, and hemodynamic shifts. Notably, a delicate equilibrium exists between hemostasis and blood fluidity, maintained by a series of regulatory mechanisms. Disturbances in this system, prompted by factors like endothelial damage or blood flow anomalies, may instigate thrombogenesis.

Given the complexity inherent to these biological systems, traditional experimental approaches may fall short in mapping the entirety of the thrombotic trajectory. Thus, computational models, anchored in fluid mechanics, biochemistry, and reaction kinetics, have been recognized as vital complementary tools.

This study leverages COMSOL Multiphysics, acknowledged for its proficiency in multidimensional simulations. The model amalgamates Navier-Stokes

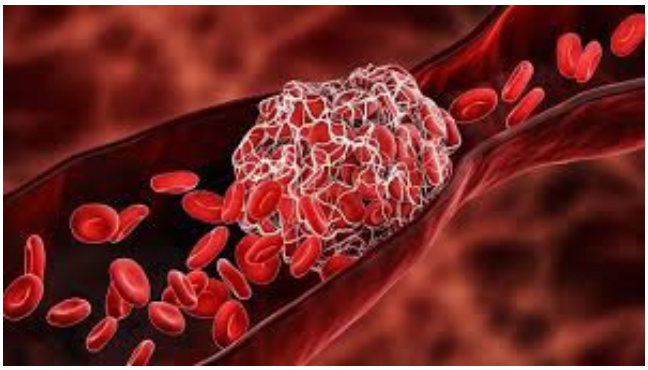

Figure 1.1: Erythrocytes within a blood vessel interrupted by a central thrombus formation.

equations, central to fluid dynamics, with the intricate biochemistry of coagulation. An innovative aspect is the consideration of fibrin-mediated viscosity adaptations, leading to an integrative method encompassing convection, diffusion, and reaction dynamics.

The potential implications of this research extend beyond theoretical realms. The insights gleaned can guide the evolution of therapeutic protocols, enabling more precise interventions for thrombotic conditions. Additionally, the findings might seed further academic inquiries, fostering the genesis of progressive, patient-centric computational models.

This thesis represents an intersection of biology and computational modeling, as we navigate through a comprehensive exploration of thrombosis, with an emphasis on harnessing simulations to decode the multifaceted mechanisms driving clot maturation.

1.2 Problem Statement and Objectives

1.2.1 Problem Statement

Thrombosis represents a complex interplay between vascular disruption, platelet activation, and fibrin deposition, a convergence commonly referred to as Virchow's triad. Current computational models tend to focus on individual aspects of thrombosis, such as hemodynamic shifts or specific biochemical pathways. However, the multifactorial nature of thrombosis demands an integrative approach. Notably, the adaptive modulation of clot rheological properties, particularly under conditions of increased fibrin concentration, remains insufficiently modeled. This identifies a clear need for an integrative computational approach to capture the multidimensional intricacies of thrombus formation.

1.2.2 Research Objectives

This study seeks to establish a comprehensive computational model via Comsol. This model intends to seamlessly combine Navier-Stokes dynamics (for vascular hemodynamics) with a biochemistry model that delineates thrombin generation and fibrin polymerization. An additional aim is to introduce convection-diffusion-reaction dynamics, offering a nuanced representation of changes in clot viscoelastic properties in relation to fibrin concentration variations.

The structured objectives for this research endeavor are:

1. Construct a Comsol-based computational framework that integrates the Navier-Stokes equations and a detailed biochemistry coagulation model.

2. Embed the convection-diffusion-reaction equations to capture the nuanced alterations in clot mechanics as a function of fibrin concentration dynamics.

3. Validate the developed model by comparison with existing experimental or clinical data to confirm its relevance and accuracy.

4. Analyze the effects of varying clot viscoelastic properties on the dynamics of thrombus formation, progression, and potential dissolution.

5. Conduct a sensitivity analysis to assess the influence of critical parameters, including hemodynamic variables, clot structure, and biochemistry kinetics, on the thrombotic process.

Through these objectives, this research aims to advance the understanding of thrombosis by bridging hemodynamics, biochemistry, and clot biomechanics, potentially informing more effective therapeutic strategies in cardiovascular care.

1.3 Research Approach

To address the research objectives outlined in the previous section, a comprehensive research approach will be adopted, combining computational modeling, numerical simulations, and data analysis. The research will be conducted in the following steps:

1. Literature Review: A thorough review of the existing literature on thrombosis simulation, computational modeling techniques, and relevant mathematical and biochemical models will be conducted. This review will provide the necessary background knowledge and help identify research gaps and limitations in the current understanding of thrombosis dynamics.

2. Model Development: The computational model will be developed using Comsol, a powerful multiphysics software package. The model will integrate the Navier-Stokes equations to capture blood flow dynamics and a biochemistry model to simulate the behavior of coagulation species. Additionally, convection-diffusion-reaction equations will be incorporated to account for clot viscosity variation when fibrin surpasses a specific threshold. The model will be constructed based on the principles established in the literature review and refined through iterative testing and validation.

3. Numerical Simulations: Once the computational model is developed, numerical simulations will be performed to investigate thrombosis dynamics. The simulations will involve varying parameters such as flow rate, clot composition, and biochemical factors to analyze their effects on clot formation, propagation, and dissolution. Multiple scenarios and conditions will be considered to explore the range of possible thrombotic outcomes and better understand the underlying processes.

4. Validation and Comparison: The developed model and simulation results will be validated against existing experimental data or clinical observations to ensure their accuracy and reliability. A quantitative comparison will be performed, analyzing key metrics such as clot size, shape, and location, as well as temporal evolution, to assess the agreement between the model predictions and the real-world observations.

5. Discussion and Conclusion: The results will be critically discussed in the context of the research objectives and the existing literature. The strengths and limitations of the computational model and simulation approach will be assessed. The implications and potential applications of the findings will be considered, along with any recommendations for further research or improvements in the model. The research will conclude with a summary of the main findings and their contributions to the field of thrombosis simulation.

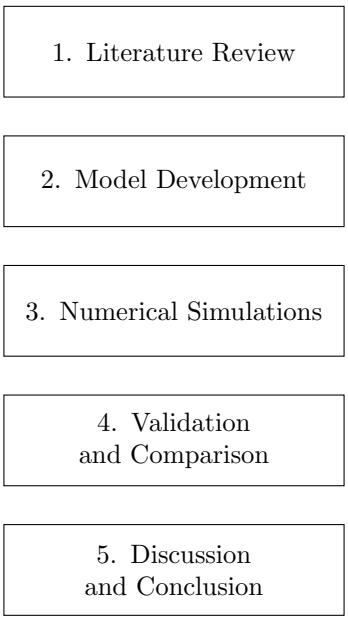

By following this research approach, we aim to develop an accurate and comprehensive computational model of thrombosis, investigate the effects of varying clot viscosity, and provide valuable insights into thrombosis dynamics. The integration of fluid dynamics, biochemistry, and convection-diffusion-reaction equations will enhance the realism and accuracy of the simulations, facilitating a deeper understanding of this complex medical condition.

Chapter 2

Theoretical Framework

2.1 Biomedical

2.1.1 Blood

Blood plays a crucial role in the human body as it facilitates the transportation of essential substances such as oxygen, carbon dioxide, nutrients, waste products, and hormones. Additionally, blood is involved in the regulation of body temperature, pH levels in tissues, and fluid volume. It also provides protection against infections and blood loss. Blood comprises various components, including erythrocytes (red blood cells), leukocytes (white blood cells), platelets, and plasma, which is predominantly composed of fluid. The diameters of these cells are approximately 7-9 μm, 10-14 μm, and 2-4 μm, respectively [14].

Due to its distinct composition, blood exhibits different properties compared to water. It has a higher density, with blood plasma having a density of 1025 kg/m^3 and erythrocytes having a density of 1125 kg/m^3 [11]. Moreover, blood has a viscosity nearly five times higher than that of water, primarily due to the presence of erythrocytes. These red blood cells account for approximately 45% of the total blood volume, known as hematocrit [14]. When the number of red blood cells increases, the viscosity of blood also rises. Figure 2.1 illustrates the consistency of blood and its components.

Erythrocytes, commonly known as red blood cells, have a vital role in the transport of gases within the body. This function is made possible by the presence of a protein called hemoglobin within erythrocytes. Hemoglobin has the ability to bind and release oxygen, enabling the transportation of gases. Leukocytes, also referred to as white blood cells, play a significant role in defending the body against various forms of damage, including bacteria, toxins, and parasites. Platelets are essential for the process of blood clotting, which is necessary when blood vessels experience rupture or damage. Further details about the coagulation process will be elaborated on in section 2.1.3.

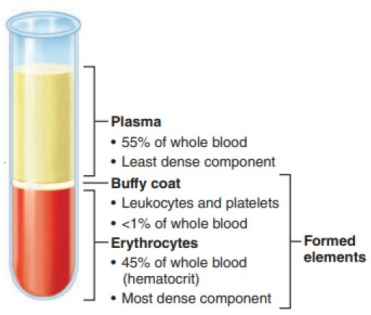

(a) Composition of blood

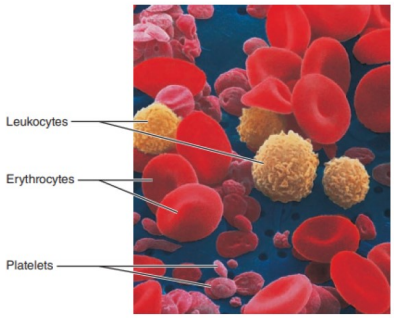

(b) Elements of blood

Figure 2.1: (a) The consistency of blood. (b) The different elements in blood imaged with SEM, magnification 1800x. [13]

2.1.2 Blood Flow

Blood circulates throughout the body via a network of blood vessels. The three primary types of blood vessels are arteries, capillaries, and veins. In the systemic circulation, arteries transport oxygenated blood towards the capillaries, where various exchanges occur, including the exchange of gases. Subsequently, the oxygen-depleted blood travels through the veins, returning to the heart and lungs. The sequential flow of blood from the artery to the capillary and then to the vein is depicted in Figure 2.2.

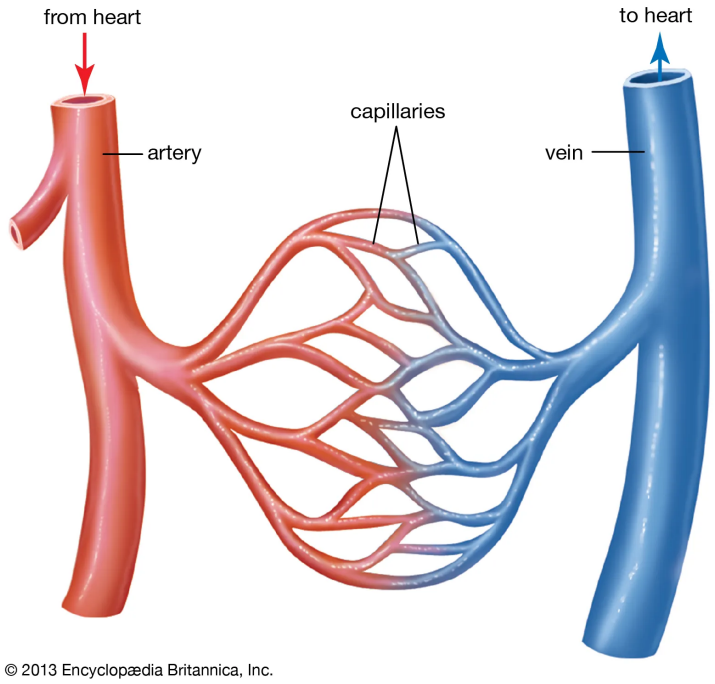

Figure 2.2: A visual representation demonstrates the movement of blood starting from an artery, passing through the capillaries, and finally reaching a vein. The capillaries play a crucial role in facilitating the exchange of gases [6].

Different types of blood vessels exhibit distinct characteristics and serve specific functions. Elastic arteries, the largest among them, have a diameter ranging from 2.5 to 1.0 cm, while the smallest capillaries can be as narrow as 9 μm [14]. Veins have an intermediate diameter, typically around 5.0 mm, although it varies depending on their location. Deep veins, which are of particular interest in this thesis regarding coagulation, have a diameter ranging from 6 to 10 mm [9].

Despite capillaries having much smaller diameters compared to large arteries like the aorta, their combined cross-sectional area allows for a significantly greater volume of blood to be accommodated. As velocity is inversely proportional to cross-sectional area [23], the blood velocity in the aorta is higher than that in the capillaries. Figure 2.3 illustrates the relationship between velocity and cross-sectional area. It is worth noting that the velocity in veins typically ranges between 10 and 30 cm/s, which can increase during systole and decrease during diastole.

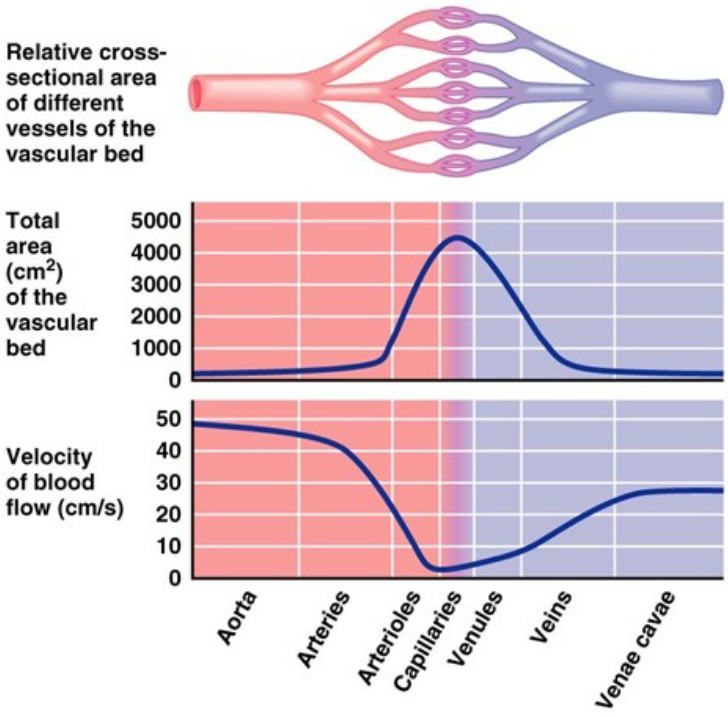

Figure 2.3: Schematic illustration depicting the interconnectedness of arteries, veins, and capillaries, highlighting how blood flow occurs through these vessels. Additionally, the figure includes two graphs illustrating the relationship between the total area (in cm^2) of a specific vessel type and the velocity of blood flow (in cm/s) [14].

2.1.3 Coagulation

Hemostasis is a complex physiological process that aims to halt blood loss. It consists of three sequential stages: vasoconstriction, platelet aggregation, and coagulation, as briefly outlined in section 2.1 and depicted in figure 2.4. Following the formation of a platelet plug at the site of injury, the intricate process of coagulation initiates. This process involves a series of intricate chemical reactions that culminate in the formation of fibrin, a substance responsible for reinforcing the platelet plug and creating a fibrin mesh. The cascade of reactions involved in coagulation is schematically represented in figures 2.4 and 2.5.

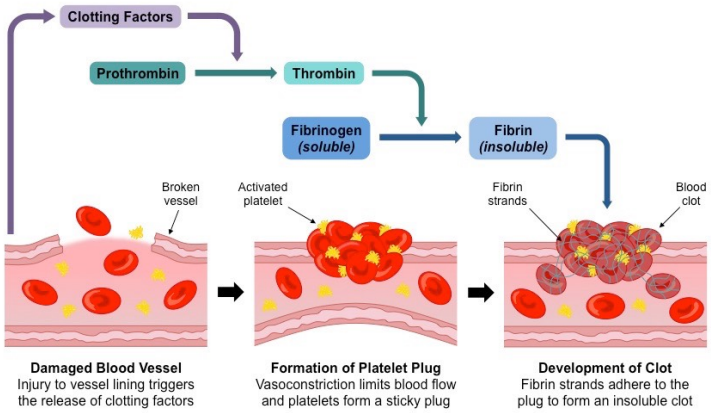

Figure 2.4: A simple visualisation of hemostasis in the blood-vessels using the extrinsic pathway. [14].

The coagulation process can be divided into three phases. The initial phase encompasses a cascade of reactions that occur just before the activation of prothrombin. Two distinct pathways, the intrinsic and extrinsic pathways, contribute to the generation of prothrombin activator. The intrinsic pathway involves clotting factors interacting with the vessel tissue, leading to the formation of prothrombin activator. On the other hand, the extrinsic pathway is triggered by the exposure of blood to the outer tissue of blood vessels, resulting in the release of Tissue Factor (TF), which initiates a separate cascade of reactions to generate prothrombin activator. Although the extrinsic pathway is more relevant in halting blood loss, thrombosis is often associated with the intrinsic pathway, particularly in the presence of inflammation.

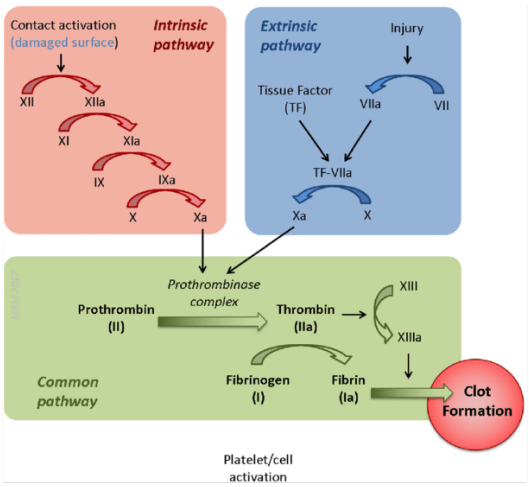

Figure 2.5: The complex coagulation pathway using various clotting factors to fibrin. Note the two pathways that reach the same result. [20].

The second phase of coagulation involves the conversion of prothrombin (II) into thrombin (IIa) with the aid of an enzyme. In the final phase, thrombin facilitates the transformation of fibrinogen into the fibrin mesh. Under normal circumstances, this process is regulated by the presence of anticoagulants, which are naturally present in higher concentrations in the blood. Consequently, the coagulation process represents a delicate equilibrium influenced by the concentrations of various species.

It is important to note that the coagulation cascade presented in this section provides a simplified representation of a more comprehensive model in which each clotting factor interacts with nearly all other factors. This more realistic model is detailed and explained in section 4.1 of the thesis.

2.1.4 Thrombosis and Embolism

The process of clot formation is vital for preventing excessive blood loss when a blood vessel sustains damage. However, the occurrence of blood clot formation in the absence of vessel damage poses a significant risk. Such clots are referred to as thrombi. When a thrombus grows to a size that obstructs circulation to a particular area, it can result in tissue death due to the lack of oxygen supply. In cases where this occurs within deep veins, it is termed deep vein thrombosis (DVT), which constitutes the primary focus of this thesis. An illustrative depiction of thrombosis is presented in Figure 2.6.

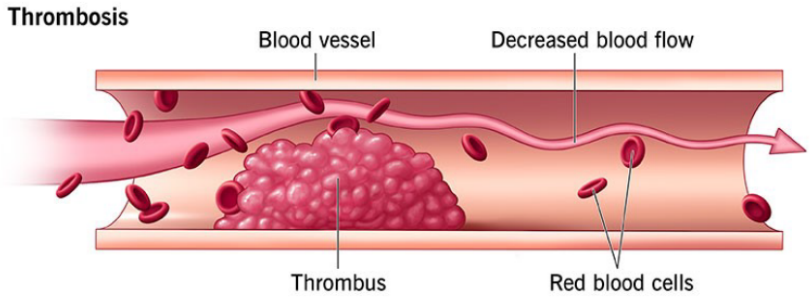

Figure 2.6: An illustration of thrombosis in a blood vessel, with a decreased blood flow after the obstruction [7].

In addition to causing vessel blockage, a portion of the thrombus has the potential to detach and travel within the bloodstream. This detached thrombus is referred to as an embolus. The embolus itself may not pose an immediate threat unless it navigates through a narrow vessel. Once lodged in such a vessel, it can create a complete blockage termed an embolism. Embolisms can occur throughout the body. For instance, if an embolus obstructs a pulmonary vessel, it severely impairs the body's capacity to receive oxygen. Similarly, an embolism in the brain can lead to a stroke, which can have fatal consequences. An illustrative representation of an embolus and an embolism is displayed in Figure 2.7.

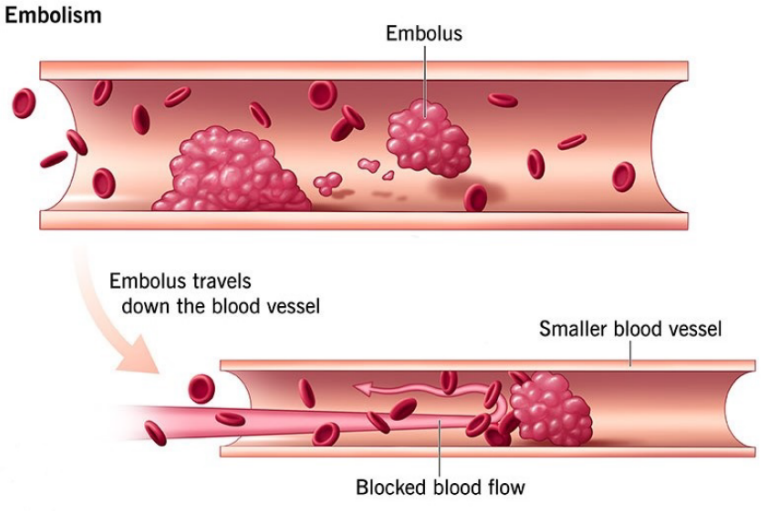

Figure 2.7: The illustration shows an embolus that is detached from the thrombus, as well as an embolism blocking an entire vessel [7].

When a patient experiences excessive clot formation due to a medical condition, it falls under the category of a thromboembolic disorder. These disorders can be attributed to three primary factors, referred to as Virchow's triad: alterations in blood flow dynamics, changes in blood properties, or irritation of the vessel wall[12]. Hemodynamic changes manifest as disruptions in blood flow, often seen in scenarios of sluggish blood circulation or stasis. Such circumstances can arise in patients confined to bed or during prolonged flights without adequate movement.

The second causative category involves modifications either in blood composition or in the process of blood coagulation. Various risk factors contribute to this, including heightened blood viscosity or the presence of the factor V Leiden mutation. Hormonal contraception also impacts blood properties, thereby elevating the risk of venous thrombosis by three to five times [13].

Vessel irritation can stem from either endothelial or vessel wall injury. In the context of this thesis, the focus lies on thrombosis caused by vessel wall injury. This type of thrombosis will be the subject of simulation in this study.

2.2 Physics

2.2.1 Navier-Stokes Equations

The Navier-Stokes equations play a fundamental role in characterizing the dynamics of fluid motion. They serve as mathematical expressions that describe the conservation of momentum for fluids, analogous to Newton's second law for solid bodies. In the context of a compressible Newtonian fluid, these equations govern and dictate the resulting behavior and motion of the fluid [3].

$$\underbrace{\rho\left(\frac{\partial \mathbf{u}}{\partial t}+\mathbf{u}\cdot\nabla\mathbf{u}\right)}_{1}=\underbrace{-\nabla p}_{2}+\underbrace{\nabla\cdot\left(\mu\left(\nabla\mathbf{u}+(\nabla\mathbf{u})^{T}\right)-\frac{2}{3}\mu(\nabla\cdot\mathbf{u})\mathbf{I}\right)}_{\mathbf{3}}+\underbrace{\mathbf{F}}_{\mathbf{4}} \tag{2.1}$$

The variables involved in the Navier-Stokes equations consist of the fluid velocity (u), fluid pressure (p), fluid density (ρ), and fluid dynamic viscosity (μ). Each term in the equations represents a distinct physical force acting on the fluid. These forces include inertial forces (1), pressure forces (2), viscous forces (3), and external forces exerted on the fluid (4). The derivation of the Navier-Stokes equations can be attributed to the collaborative efforts of Navier, Poisson, Saint-Venant, and Stokes, spanning the years between 1827 and 1845.

These equations are always solved together with the continuity equation:

$$\frac{\partial \rho}{\partial t}+\nabla\cdot(\rho\mathbf{u})=0 \tag{2.2}$$

The Navier-Stokes equations represent the conservation of momentum, while the continuity equation represents the conservation of mass.

In this thesis, the simulation focuses on modeling blood flow. It is assumed that blood behaves as an incompressible fluid, which implies a constant density (ρ). Consequently, the divergence of the velocity vector ($\nabla \cdot \vec{u}$) is zero. This assumption simplifies the Navier-Stokes equation (2.1) to:

$$\rho \left(\frac{\partial \mathbf{u}}{\partial t} + \mathbf{u} \cdot \nabla \mathbf{u} \right) = -\nabla p + \mu \nabla^2 \mathbf{u} + \mathbf{F} \tag{2.3}$$

These equations all together form the foundation of fluid flow modeling. By solving these equations with specific boundary conditions, such as inlets, outlets, and walls, one can predict the velocity and pressure of the fluid within a given geometry. Due to their intricacy, the equations have only a limited number of analytical solutions. For simpler cases like flow between parallel plates or in a circular pipe, solving these equations is relatively straightforward. However, for more intricate geometries, the equations require advanced techniques. Several methodologies come to the fore in this context:

Numerical methods like Finite Difference Method (FDM), Finite Element Method (FEM), Finite Volume Method (FVM), and Boundary Element Method (BEM) offer computer-based solutions. Semi-analytical methods, such as perturbation techniques and similarity solutions, merge analytical and numerical methods to address specific challenges. For real-world insights, experimental methods, including Particle Image Velocimetry (PIV) and Laser Doppler Anemometry (LDA), provide empirical data. Moreover, advanced simulations using Direct Numerical Simulation (DNS) can directly solve Navier-Stokes without resorting to turbulence models, albeit at a high computational cost. Large Eddy Simulation (LES) and Reynolds-Averaged Navier-Stokes (RANS) Equations, on the other hand, offer avenues to model turbulent flows. The Lattice Boltzmann Method (LBM) offers a kinetic perspective by simulating discrete particle motion on a lattice.

Selecting the right method hinges on the problem's specifics, the precision required, the computational resources available, and the geometry's intricacies.

2.2.2 Convection-Diffusion-Reaction Equations

To model the evolution of species concentrations c_i in a system, the advection-diffusion-reaction equation is employed. This equation, derived using a continuity formulation similar to equation (2.2), incorporates the production or consumption rate of the species as follows:

$$\frac{\partial c_i}{\partial t} + \nabla \cdot \vec{j} = R_i \tag{2.4}$$

Here, $\vec{j}$ represents the total flux of the species, and R denotes the net production term for c_i resulting from chemical reactions. The total flux term, $\vec{j}$, encompasses both a diffusion component, j_{diff}, and an advection component, j_{adv}, associated with flow transport. The diffusion term is governed by Fick's first law of diffusion:

$$\vec{j}_{diff} = -D_i \nabla c_i \tag{2.5}$$

where D represents the diffusion coefficient of the corresponding species. The advective flux is given by:

$$\vec{j}_{adv} = \vec{u} c_i \tag{2.6}$$

where $\vec{u}$ denotes the velocity vector. By substituting $\vec{j} = j_{diff} + j_{adv} = -D_i \nabla c_i + \vec{u} c_i$ into equation (2.4), the advection-diffusion equation is obtained:

$$\frac{\partial c_i}{\partial t} + \nabla \cdot (-D_i \nabla c_i + \vec{u} c_i) = R_i \tag{2.7}$$

Under the assumption of a no-slip boundary condition at the wall ($\vec{u} = 0$), equation (2.7) can be simplified as:

$$\frac{\partial c_i}{\partial t} + \nabla \cdot (-D_i \nabla c_i) = R_i \tag{2.8}$$

This equation implies that the convective (or advective) flux of species c_i due to the fluid's velocity is zero at the wall, as a direct consequence of the no-slip boundary condition which states that $\mathbf{u} = 0$ at the wall. Therefore, only the diffusive transport, governed by the term $-D\nabla c_i$, contributes to the species transport at the wall.

However, while equation (2.8) captures the transport of species c_i in the fluid domain due to diffusion, it does not inherently provide insights into potential reactions or other interactions the species might have at the wall. For instance, species could be adsorbed, react, or desorb from the wall, which would require additional boundary conditions or terms in the model.

It is also worth mentioning that the term R_i in equation (2.8) represents the net production or, perhaps more aptly termed, the consumption rate of the species within the fluid domain. This term encompasses all the reactions the species might undergo within the fluid, but, as currently formulated, it does not provide specific details about reactions occurring right at the wall interface.

To ensure a holistic and realistic modeling of species transport, it's crucial to also define boundary conditions specific to each chemical species when considering more intricate scenarios involving species-wall interactions. Such details, however, are outside the scope of our current model and would be an avenue for further research or refinement based on specific applications.

2.2.3 Viscosity of Blood

The viscosity term in equation (2.1) holds significant importance. Unlike water, blood exhibits non-normal behavior in fluid flow. Its physical properties vary depending on the shear rate ($\dot{\gamma}$), which represents the velocity gradient. This behavior is referred to as non-Newtonian, as the fluid properties change with varying flow rates and shear rates. This concept falls under the field of rheology. Extensive research has been conducted on different types of non-Newtonian fluids and their relationship with viscosity and shear rate. Examples include Bingham fluids, Power-law liquids, Casson liquids, Carreau model, and Carreau-Yasuda model. In this thesis, a modified version of the Carreau-Yasuda model [10] is employed.

The original Carreau-Yasuda fluid is described by the following equation:

$$\mu(\dot{\gamma}) = \mu_\infty + (\mu_0 - \mu_\infty)\left[1 + (\lambda\dot{\gamma})^a\right]^{\frac{n}{a}} \tag{2.9}$$

In this equation, μ represents the viscosity dependent on $\dot{\gamma}$, μ_∞ is the viscosity at extremely high (asymptotically infinite) shear rates, μ_0 is the viscosity at zero shear rate, λ is the relaxation time, and n and a are fitting parameters obtained from literature or experimental data. Although equation (2.9) can be related to a Carreau fluid for fluids with different non-Newtonian properties by setting $a = 2$, this thesis employs a modified version:

$$\mu(\dot{\gamma}) = \mu_1 m(\epsilon_{rbc})\left[1 + (\lambda_1\dot{\gamma})^2\right]^{\frac{n(\epsilon_{rbcc})}{2}} \tag{2.10}$$

In this modified equation, μ_1 is a conversion factor of 0.001 to obtain SI units, λ_1 represents the relaxation time of $0.11[s/m]$, n is a function dependent on the hematocrit ϵ_{rbc} in the blood, as explained in section 2.1. The term within the square brackets can be rewritten as a dimensionless shear rate $\bar{\gamma} = 1 + (\lambda_1\dot{\gamma})^2$. Additionally, this reduced model is fitted for improved performance at low shear rates, with the fitting parameter a having a value of 0.0068, which is used to shift the shear rate:

$$\mu(\dot{\gamma}) = \mu_1 m(\epsilon_{rbc})\left[1 + (\lambda_1(\dot{\gamma} + a))^2\right]^{\frac{n(\epsilon_{rbcc})}{2}} \tag{2.11}$$

A general assumption is made that erythrocytes constitute 45% of the total blood volume, denoted as $\epsilon_{rbc} = 0.45$. This value affects the functions m and n provided below [5] [24]:

$$n = k_0(-0.8913\epsilon_{rbc}^3 + 2.0679\epsilon_{rbc}^2 - 1.7814\epsilon_{rbc}) \tag{2.12}$$

$$m = 70.782\epsilon_{rbc}^3 - 22.454\epsilon_{rbc}^2 + 9.7193\epsilon_{rbc} + 1 \tag{2.13}$$

The value of k_0 is determined based on the dimensionless shear rate $\overline{\dot{\gamma}}$ in the equation given below:

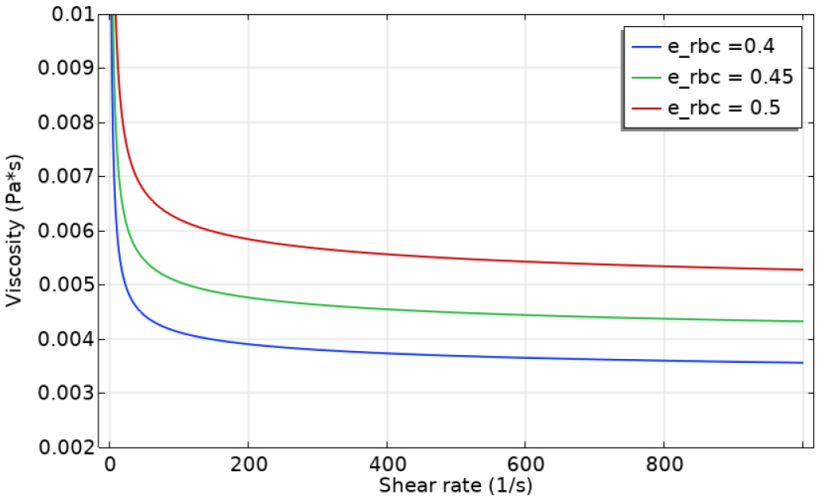

Figure 2.8: Viscosity of blood as a function of shear rate $\dot{\gamma}$ for different hematocrits ϵ_{rbc}.

$$k_0 = \frac{\ln(\ln(\overline{\dot{\gamma}}))}{\ln(\dot{\dot{\gamma}})} \tag{2.14}$$

Figure 2.8 illustrates the relationship between the hematocrit ϵ_{rbc} and the viscosity calculated using the modified Carreau-Yasuda equation (2.10).

2.2.4 Reynolds Number

Another parameter that describes flow is the dimensionless Reynolds number which is the ratio between the inertial forces and the viscous forces:

$$Re = \frac{\text{inertial forces}}{\text{viscous forces}} = \frac{\rho \bar{u} D/2}{\bar{\mu}} \tag{2.15}$$

With ρ the density of the fluid, $\bar{u}$ and $\bar{\mu}$ being the average velocity and viscosity respectively and D is a characteristic length for the geometry, for example the width D of a channel. This number is used as an indicator for the flow characteristics like laminar or turbulant flow. If $Re < 2000$, the fluid generally is a laminar flow. The blood flow in the microchannel in this thesis has a Reynolds number of around $Re = 0.023$, so it has laminar flow.

Chapter 3

Methodology

3.1 Biochemistry Models for Coagulation Species

To simulate the coagulation model, a further and deeper understanding of the governing chemical reaction systems during coagulation is needed.

3.1.1 Simplified 1-Species Coagulation Model

The one-species coagulation model, with its emphasis on fibrin, provides a simplified yet foundational framework to understand the complex process of coagulation. Acting as a stepping stone, it offers a distilled view of clot formation before delving into multi-species models like the Bodnar Simplified 7-Species Coagulation Model.

Fibrin is pivotal in clotting. Originating from fibrinogen through enzymatic actions, its polymerization is integral to clot formation and stabilization. The one-species model encapsulates the dynamics around fibrin to depict the essence of clot development.

Table 3.1 depicts the diffusion constant and inward flux related to fibrin in the model's context.

Table 3.1: Diffusion constant D and inward flux J_o, c of fibrin in the one-species model.

Species	**Name**	$D[\mathrm{m}^2/\mathrm{s}]$	$J_o, c[\mathrm{mol}/\mathrm{m}^2 \cdot \mathrm{s}]$
Ia	Fibrin	2.47×10^{-11}	$5E-10$

While fibrin doesn't have a reaction rate in this model, its flux, which represents its movement and accumulation at the boundary, is crucial.

Transitioning from this rudimentary model, we recognize the need for intricate frameworks like the Bodnar Simplified 7-Species Coagulation Model. This need stems from the myriad of processes inherent in real-world coagulation. Progressing from a singular focus on fibrin to embracing a multi-species perspective

is a vital evolution, shedding light on the broader coagulation landscape. Future sections will delve into this expanded view, unpacking the intricacies of coagulation dynamics in more depth.

3.1.2 Papadopoulos-inspired 4-Species Coagulation Model

This section presents a patient-specific mathematical model derived from Papadopoulos' work [18], refined for accurate representation of thrombin generation dynamics within computational fluid dynamics (CFD) simulations. Built upon carefully selected equations, this model encapsulates the intricacies of coagulation reactions, enabling precise prediction of thrombin generation over time. Calibration is achieved by adjusting coefficients to fit experimental thrombin generation assay data.

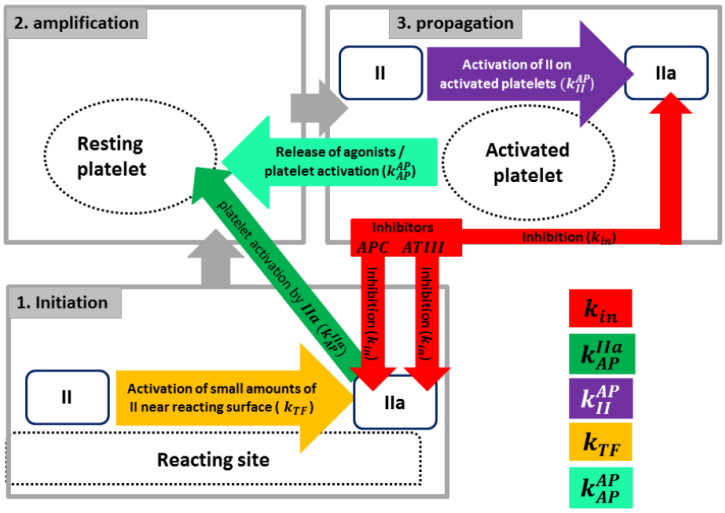

Figure 3.1: Schematic of the reduced cell-based coagulation model for the thrombin sub-model development. [17]

Empirical evaluations emphasize the model's fidelity, particularly in varying platelet concentrations, illustrating consistent agreement with experimental observations. The model's robustness is further underscored by its ability to achieve a balance between complexity and computational efficiency, making it ideal for scenario-specific coagulation simulations.

Subsequent sections detail the integration of this thrombin generation model into CFD simulations, including its foundational equations, boundary conditions, and numerical methodologies. Collectively, these components facilitate a nuanced understanding of the relationship between thrombin generation and fluid dynamics across diverse scenarios.

In summary, this model stands as a pivotal contribution to the simulation and understanding of blood coagulation dynamics, offering a balance between

intricacy and efficiency.

Table 3.2: Concentration values c and diffusion constants D for species in blood [18].

Species	Name	$D[\mathrm{m}^2/\mathrm{s}]$	c[nM]
IIa	Thrombin	4.16×10^{-11}	1400
II	Prothrombin	3.32×10^{-11}	0
AP	Activated Platelets	2.5×10^{-11}	0
RP	Resting Platelets	2.5×10^{-11}	70000

Table 3.3: Parameters for the differential equations [18].

Parameter	Value
k_{in}	0.0262 [1/s]
k_{surf}	7.223×10^{-2} [1/s]
k_{AP}^{AP}	5.24×10^{-2} [1/s]
k_{II}^{AP}	0.525 $[\mathrm{m}^3/mol/s]$
k_{AP}^{IIa}	0.002 [1/s]

Table 3.4: Original system of differential equations [18].

Substance	Source term
Thrombin [IIa]	$\frac{\partial [IIa]}{\partial t} = -k_{\mathrm{in}}[IIa] + (k_{\mathrm{surf}} + k_{II}^{AP} \cdot [AP]) \cdot [II]$
Prothrombin [II]	$\frac{\partial [II]}{\partial t} = -(k_{\mathrm{surf}} + k_{II}^{AP} \cdot [AP]) \cdot [II]$
Activated Platelets	$\frac{\partial [AP]}{\partial t} = k_{AP}^{AP} \cdot [AP] \cdot [RP] + k_{AP}^{IIa} \cdot [RP]$
Resting Platelets	$\frac{\partial [RP]}{\partial t} = -k_{AP}^{AP} \cdot [AP] \cdot [RP] - k_{AP}^{IIa} \cdot [RP]$

Thrombin (IIa)

Thrombin (IIa) concentrations are steered by equations delineating its synthesis and degradation rates. Terms such as the kinetic formation rate k_{in} and surface-initiated reactions via activated platelets k_{surf}, along with the thrombin-antiplasmin interaction $k_{\mathrm{AP\_II}}$, dictate its behavior.

Prothrombin (II)

Prothrombin (II) concentrations are tied to thrombin via reversible pathways. Surface reactions, dictated by k_{surf} and $k_{\mathrm{AP\_II}}$, govern prothrombin's conversion dynamics to thrombin.

Activated Platelets (AP)

Activated platelets (AP) engage in kinetic exchanges with resting platelets (RP), modulating thrombin generation. Their synthesis rate is defined by $k_{\mathrm{AP\_AP}}$

and RP concentrations, while their interaction with thrombin is determined by $k_{\text{IIa\_AP}}$.

Resting Platelets (RP)

Resting platelets (RP) undergo reversible interactions with AP, influencing thrombin generation's broader dynamics. The rate constants $k_{\text{AP\_AP}}$ and $k_{\text{IIa\_AP}}$ govern these interactions, modulating thrombin concentrations.

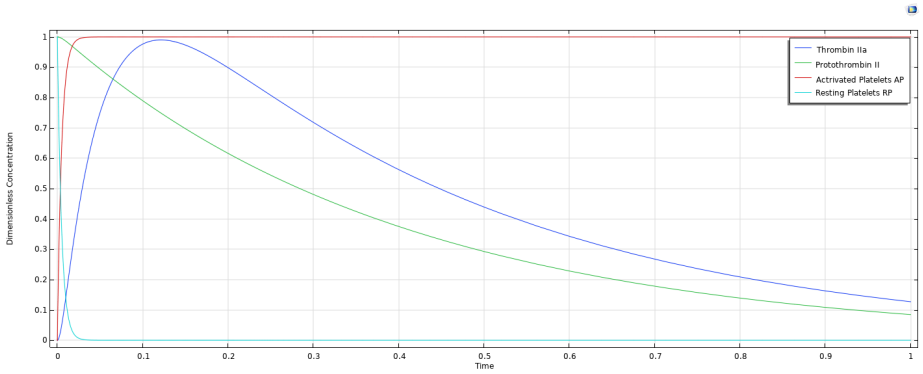

Figure 3.2: Dimensionless species development corresponding to the initial conditions of the coupled model.

In the process of deriving the normalized system from the original one, we primarily employed the normalization technique, which entails the introduction and application of scaling factors to the system of differential equations. Specifically, scaling or normalization factors were introduced for each key variable, represented by maximum or steady-state values, namely: $[IIa]_{\max}$ for Thrombin [IIa], $[II]_{\max}$ for Prothrombin [II], $[AP]_{\max}$ for Activated Platelets, and $[RP]_{\max}$ for Resting Platelets. New normalized variables were then defined by dividing each original variable by its respective scaling factor, resulting in dimensionless entities such as $[IIa]_{\text{new}} = \frac{[IIa]}{[IIa]_{\max}}$. Substituting these new variables into the original system introduced terms with scaling factors in the equations. Further, using differential properties concerning time, the source terms in the normalized system were derived from the original system's source terms. These normalized equations, expressed in terms of the normalized variables and scaling factors, often present a more simplified or tractable form, with values typically spanning between 0 and 1, thereby rendering the system more analytically convenient. The Normalized system can be seen below in Table 3.5.

The synthesis of these reactions within the model provides a holistic platform for examining coagulation factor interactions, platelet activity, and thrombin synthesis, forming the substrate for subsequent CFD simulations and facilitating an intricate understanding of thrombin generation in diverse contexts.

Table 3.5: Normalized system of differential equations.

Substance	Source term
Thrombin [IIa]	$-k_{\text{in}} \cdot [IIa] + (k_{\text{surf}} + k_{\text{AP\_II}} \cdot [AP] \left(\frac{\text{APmax}}{\text{APnew}}\right)) \cdot [IIa] \left(\frac{\text{IImax} \cdot \text{IIanew}}{\text{IIamax} \cdot \text{IInew}}\right)$
Prothrombin [II]	$-(k_{\text{surf}} + k_{\text{AP\_II}} \cdot [AP] \left(\frac{\text{APmax}}{\text{APnew}}\right)) \cdot [II]$
Activated Platelets	$k_{AP\_AP} \cdot [AP] \cdot [RP] \left(\frac{RP_{\text{max}}}{RP_{\text{new}}}\right) + k_{IIa\_AP} \cdot [RP]$
Resting Platelets	$-k_{AP\_AP} \cdot [AP] \cdot [RP] \left(\frac{AP_{\text{max}}}{AP_{\text{new}}}\right) - k_{IIa\_AP} \cdot [RP]$

3.1.3 Bodnar Simplified 7-Species Coagulation Model

In order to simulate the coagulation model effectively, it's imperative to grasp the chemical reactions foundational to coagulation. While earlier chapters introduced a basic model, this chapter transitions to a more nuanced version, as articulated in [22]. For a comprehensive understanding, the coagulation model from [21] serves as an ideal reference. However, due to computational limitations, we've chosen to work with the intermediate model studied in previous thesis [22] [16]. This chapter will also explore the essential blood properties for clot simulation and provide insights into the set boundary conditions.

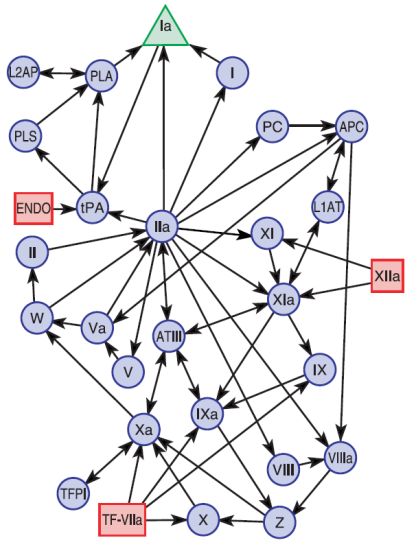

Figure 3.3: The full coagulation model [21]. The red boxes are not part of the 25 species, but represent free parameters. The green triangle is the end product: fibrin.

The current model involves a significant number of species to be solved for in the advection-diffusion equation (2.7). However, this poses computational challenges, particularly when dealing with patient-specific geometries, as it would

result in excessively high computational costs. To address this issue and improve simulation feasibility, it is necessary to reduce the number of dependent species. Consequently, the model depicted in figure 3.1 can be simplified to a 7-species model, as described in [22] and [16]. The seven species involved in the simplified model are:

1. Fibrinogen
2. Fibrin
3. Thrombin (IIa)
4. Anti-Thrombin
5. tPA (Tissue Plasminogen-Activator)
6. Plasminogen
7. Tissue Plasminogen Activator

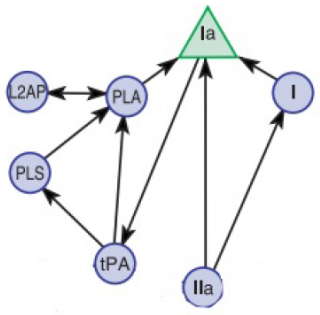

Figure 3.4: The intermediate model of the coagulation process, including 7 species [21]. The goal of the process is the production of fibrin, indicated with Ia..

The original 25-species coagulation model has been simplified and reduced to a 7-species model. The schematic representation of this simplified model can be observed in figure 3.2. To account for the absence of certain connections with other species during inflammation, fixed values for thrombin (IIa) and tissue Plasminogen-Activator (tPA) are used. The treatment of these fixed values and their incorporation into the boundary conditions is discussed. The values and diffusion constants for each species, which are consistently present in healthy blood, can be found in table 3.1 [21].

The species dynamically react with every other species. So, there is a continuous production and consumption rate Ri. The reaction rates can be found in table 3.2 and the corresponding rate parameters can be found in table 3.3.

Table 3.6: Values of the concentrations c and diffusion constants D of the different species always present (or not present) in blood.

Species	Name	$D[\mathrm{m}^2/\mathrm{s}]$	c[nM]
I	Fibrinogen	3.10×10^{-11}	7000
Ia	Fibrin	2.47×10^{-11}	0
IIa	Thrombin	6.47×10^{-11}	0
L2AP	AntiPlasmin	5.25×10^{-11}	105
PLA	Plasmin	4.93×10^{-11}	0
PLS	Plasminogen	4.81×10^{-11}	2180
tPA	Tissue Plasminogen Activator	5.28×10^{-11}	0.08

Table 3.7: Species and their respective reaction rates [22].

Species	Reaction rate R_i
I	$-\frac{k_1[IIa][I]}{K_{1M}+[I]}$
Ia	$\frac{k_1[IIa][I]}{K_{1M}+[I]} - \frac{h_1[PLA][Ia]}{H_{1M}+[Ia]}$
L2AP	$-h_{PLA}[PLA][L2AP]$
PLA	$\frac{k_{PLA}[PPA[PLS]}{K_{PLAM}+[PLS]} - h_{PLA}[PLA][L2AP]$
PLS	$-\frac{k_{PLA}[tPA][PLS]}{K_{PLAM}+[PLS]}$

Table 3.8: Rate parameters and their values [22].

Rate parameters	Value	Unit
k_1	59	s^{-1}
K_{1M}	$3.16 \cdot 10^{-3}$	$\mathrm{mol/m}^3$
h_1	25	s^{-1}
H_{1M}	0.25	$\mathrm{mol/m}^3$
h_{PLA}	1600	$\mathrm{m}^3/(\mathrm{s} \cdot \mathrm{mol})$
k_{PLA}	0.2	s^{-1}
K_{PLAM}	$1.8 \cdot 10^{-5}$	$\mathrm{mol/m}^3$

3.2 Properties of Blood

The properties of blood are not constant. Blood is a non-Newtonian fluid. Its viscosity depends on the shear rate, and its density depends on the concentration of red blood cells. Blood consists of approximately 55% plasma and 45% erythrocytes, resulting in an average density given by the following equation:

$$\rho_{\text{avg}} = (1 - \epsilon_{\text{rbc}}) \cdot \rho_{\text{plasma}} + \epsilon_{\text{rbc}} \cdot \rho_{\text{rbc}} \tag{3.1}$$

Here, ρ_{plasma} represents the density of blood plasma, ρ_{rbc} represents the density of erythrocytes, and ϵ_{rbc} represents the hematocrit, as discussed in section 2.1. The hematocrit values can be adjusted for different patients.

The concentration of erythrocytes in blood can be estimated using the following formula:

$$c_{\text{rbc}} = \frac{5 \times 10^{15}[\text{cells/m}^2]}{N_A[1/\text{mol}]} \tag{3.2}$$

The values are approximated to be in the range of $4.2 - 5.4 \times 10^{15}$ cells per m^2 for males and $4.7 - 6.1 \times 10^{15}$ cells per m^3 for females [15], and N_A is the Avogadro constant of 6.022×10^{23} per mol.

A diffusion coefficient of $\mathbf{D} = 3.4 \times 10^{-12}\,\mathrm{m}^2/\mathrm{s}$, corresponding to hemoglobin [4], is used.

3.3 Clot Viscosity Variation Method: A Simple Approach to Simulate Complex Phenomena

One of the central innovations in this thesis lies in our approach to model a highly intricate phenomenon, thrombus formation, using a simple yet effective method. Thrombus formation within blood vessels is a multifaceted process characterized by the interaction of various biochemical species, and capturing its dynamics typically demands complex computational models. However, in this work, we introduce a novel strategy that simplifies this complexity while retaining the essential characteristics of thrombus-induced changes in blood flow.

Our methodology centers on simulating the effect of clot formation on blood flow velocity by modulating blood viscosity through a step function. This step function allows us to introduce a clot-related viscosity increase in a straightforward manner, significantly reducing the computational complexity compared to traditional approaches.

The mathematical foundation of this method relies on a viscosity-modifying step function defined as:

$$\mu_{\text{blood}} = \begin{cases} \mu_{\text{blood}} & \text{if } c_{\text{fibrin}} \leq c_{\text{crit}} \\ b \cdot \mu_{\text{blood}} & \text{otherwise} \end{cases} \tag{3.3}$$

In this equation, μ_{blood} represents the viscosity of blood, c_{fibrin} signifies the fibrin concentration, c_{crit} denotes the threshold value beyond which viscosity increases, and b is the amplification factor. Notably, the choices of b as 100 and c_{crit} as 50 nM aligns with established references [22] [16]. These parameters are adaptable to tailor the model for specific scenarios. In our study encompassing three distinct biochemical models, we standardized the values as follows: for all three models, we set 'b' to 1000, while c_{crit} was approximated at around 20% of the maximum thrombogenic species concentration.

Furthermore, to ensure a smooth transition, we introduce a transition zone to slightly taper the step function. This approach elegantly simplifies the intricate thrombus-induced viscosity variations while preserving their critical role in modulating blood flow.

This innovative strategy forms the cornerstone of our research, demonstrating that complex biological phenomena can be effectively simulated and analyzed using streamlined computational methods. By reducing computational complexity without compromising the essential characteristics of the phenomenon, we pave the way for a deeper understanding of thrombus-related dynamics under varying conditions. In the subsequent chapters, we delve into the implementation of this method and its implications, ultimately advancing our knowledge of thrombus formation and its impact on blood flow.

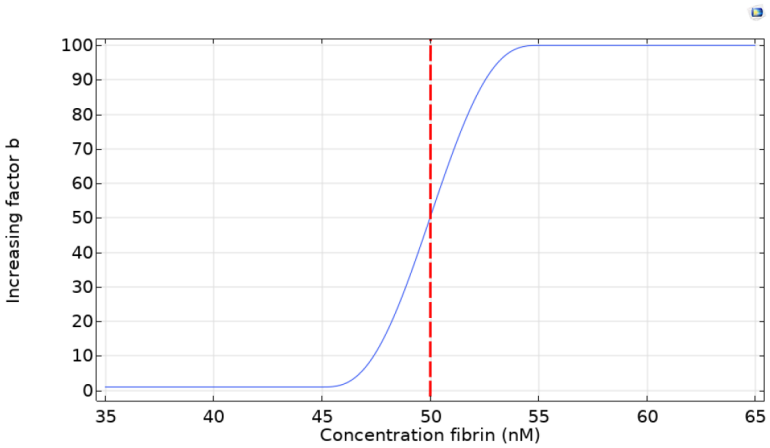

Figure 3.5: The smoothed step-function used for the increase in viscosity. The red dashed line marks the threshold value c_{crit}.

3.4 Numerical Methods and Simulation

Comsol Multiphysics 5.6 was used for the simulations of this thesis. To simulate fluid flow and thrombosis generation computationally, it is needed to have a numerical method that can solve these differential equations and geometries in which these physical phenomena occur. Next to that are the different ways to mesh a geometry that affect the results.

3.4.1 Finite Element Method

In order to solve the (partial) differential equations governing physical phenomena, numerical methods are employed. Among these methods, the Finite Element Method (FEM) is utilized within the scope of this thesis. This computational approach is implemented through simulation software, specifically COMSOL [1]. The Finite Element Method solver is constructed by discretizing the domain where the differential equations are applicable. This discretization is achieved through the creation of mesh elements, as illustrated in various forms in Figure 3.6 each suited for distinct scenarios. In this thesis, the choice has been made to employ tetrahedrals as the discretization elements.

Now, utilizing these small elements, the differential equations can be effectively solved. One approach involves transforming the differential equation, such as the analytical Navier-Stokes equation, also referred to as the strong form, into an integral equation known as the weak form. This transformation is achieved by multiplying the equation by a test function ϕ and integrating it over a specific domain Ω in which the equation is valid. The strong form assumes that all terms in the differential equation are well-defined across the entire applicable domain. In contrast, the weak form only necessitates that the

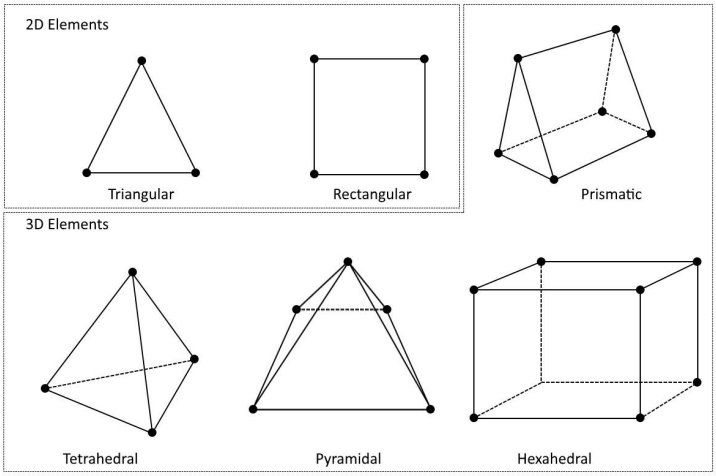

Figure 3.6: The different meshing elements that can be used. Only the tetrahedral elements are used. [1]

integral equality holds. When this formulation is applied to equation (3), which is three-dimensional and thus needs to be integrated over a volumetric domain, it results in the following weak form:

$$\begin{aligned} &\int_V \rho \frac{d\vec{u}}{dt} \cdot \phi \, d\vec{V} + \int_V (\rho \vec{u} \cdot \nabla \vec{u}) \cdot \phi \, d\vec{V} \\ &\quad = -\int_V \left(\nabla p + \nabla \cdot \left(\mu \left(\nabla \vec{u} + (\nabla \vec{u})^T \right) \right) \right) \cdot \phi \, d\vec{V} + \int_V \vec{F} \cdot \phi \, d\vec{V} \end{aligned} \tag{3.4}$$

In situations where the equation must hold for all test functions ϕ, the utilization of small volume mesh elements becomes crucial for solving this equation. Both the test functions ϕ and the solutions to these differential equations belong to Hilbert space, a vector space that enables convenient manipulation of these functions. This characteristic allows us to treat the solutions as linear combinations of specific functions, analogous to how vectors function in linear algebra. As a result, we can derive approximate solutions by transforming the weak form into a system of non-linear equations and subsequently solving this system.

Furthermore, the solver handles these equations using matrices. Due to the numerous sets of non-linear equations involved, the matrices can become exceptionally large. To tackle this challenge, software tools like COMSOL employ MUMPS (MUltifrontal Massively Parallel Solver) [2]. This solver employs the Gaussian elimination algorithm, also known as Row reduction, to solve these linear equations in the form of $Ax = b$. The simulation also makes use of the generalized minimal residual cost as an iterative solver. The idea is that

the residual or the error is minimized to find the approximated solution to the problem.

3.4.2 Geometry and Meshing

The main objective of this thesis is to validate the viscosity variation model for simulating thrombosis and compare it among three different biochemistry systems.

Microfluidic Device

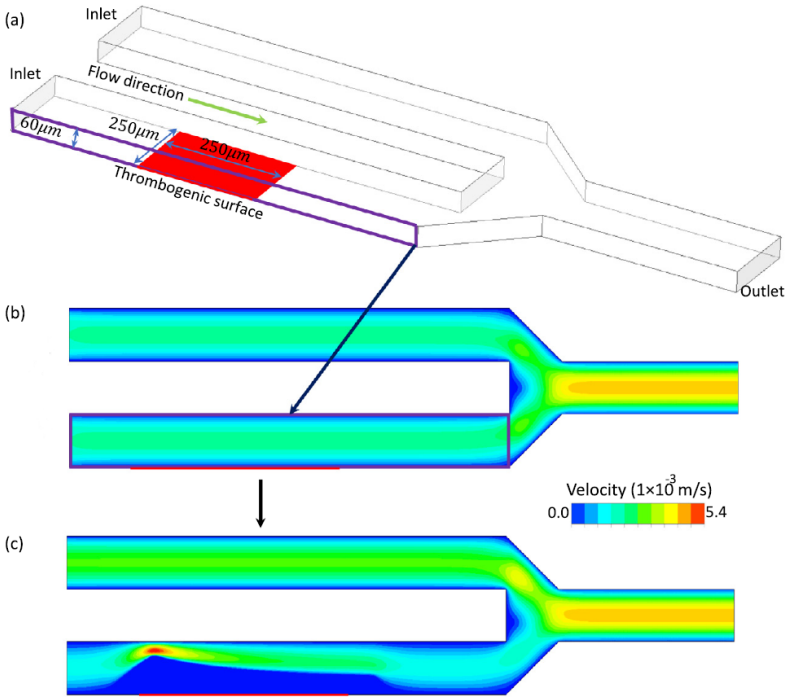

Figure 3.7: 3D representation of the microfluidic device used in previous experiments [8, 12]. The microfluidic channel dimensions are $250 \times 60\,\mu$m, allowing for a 2D flow approximation due to the substantial depth-to-height ratio.

To validate our model's accuracy, we simulated thrombus formation within a microfluidic channel. It consists of two rectangular channels merging into a single outlet, as shown in Figure 3.7. We adopted a 2D geometry approximation consistent with previous research [19].

Mesh Independence Analysis

In addition to the computational models described earlier, this study employed three-dimensional (3D) simulations to further enhance the robustness of our conclusions. These 3D simulations provided an extra dimension of insight into the coagulation dynamics within the complex geometries of the blood vessels. This subsection focuses on the mesh independence analysis conducted to determine the optimal mesh resolution for accurate simulations while comparing fibrin concentration at various critical points within the domain. This analysis enhances result reliability and highlights the model's sensitivity to mesh size, offering insights into spatial and temporal variations in fibrin concentration.

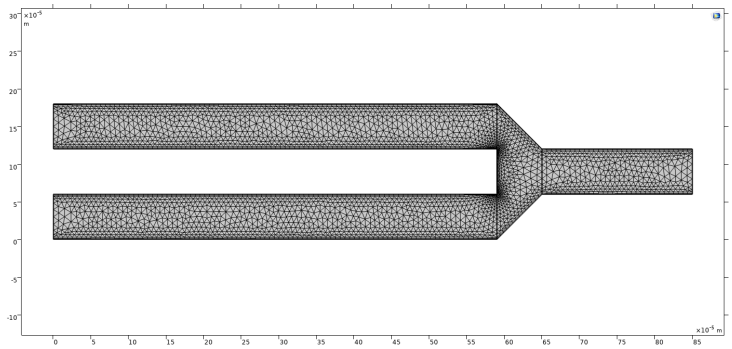

Figure 3.8: Two-dimensional mesh discretization generated by the COMSOL 5.6 mesher - Normal Element size setting.

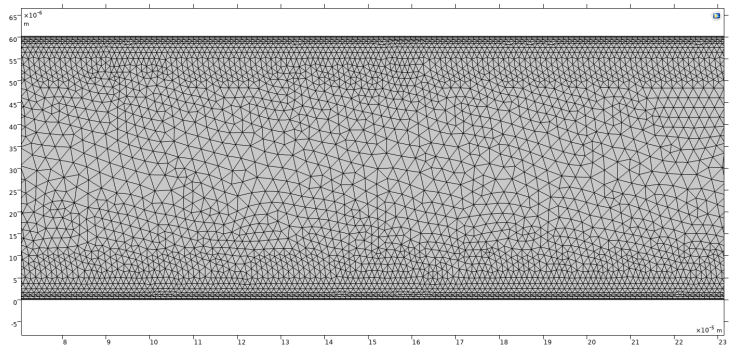

Figure 3.9: Detail of two-dimensional meshing near the inflammation boundary - Extra Fine Element size setting.

Table 3.9 provides insights into our computational simulations, detailing geometry and mesh characteristics for both 2D and 3D simulations. This table allows us to assess the impact of mesh quality and refinement on the reliability of our research findings.

Table 3.9: Geometry and Mesh Details for 2D and 3D Simulations

Geometry	Domain el.	Edge el.	Avg. el. quality
2D Normal	5998	578	0.8102
2D Finer	27125	1475	0.781
2D Ex. Fine	73505	2804	0.8016
3D Normal	240585	1131	0.6845
3D Finer	2106770	2571	0.6942
3D Ex. Fine	9433170	4580	0.6944

The mesh independence analysis involved comparing fibrin concentration at various locations within the domain for different mesh resolutions. Figure 3.10 illustrates the conditions at a location representing 1% of the entire distance from the center of the inflammation region to the upper channel boundary. Upon close examination, it becomes evident that the variations in development are relatively minor across all mesh sizes, with a slightly more pronounced distinction observed in the finer and extremely fine meshes. Consequently, the finer mesh was ultimately selected for further analysis, as it strikes a balance between computational efficiency and result accuracy.

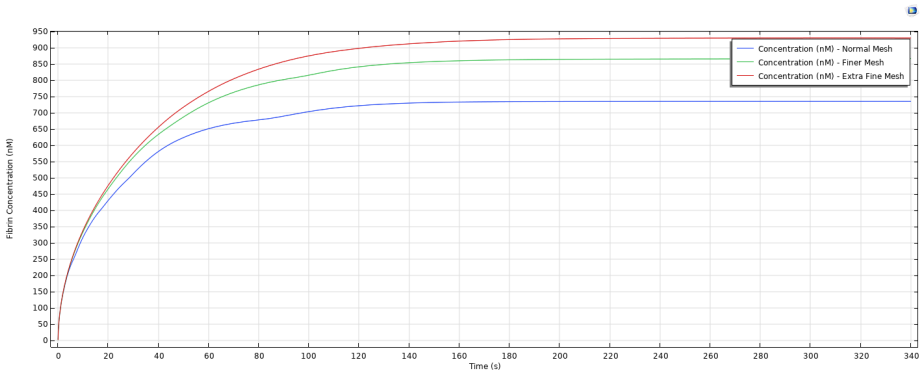

Figure 3.10: Mesh comparison for the 1% point.

3.4.3 High-Performance Computing (HPC)

High-Performance Clusters (HPC) represent cutting-edge computing infrastructures meticulously designed to efficiently manage intricate and computationally demanding tasks. These clusters comprise interconnected computers and processors operating collaboratively to execute parallel processing tasks, rendering them exceptionally well-suited for scientific simulations and data-intensive computations.

In the context of this study, the computational work was conducted on the High-Performance Cluster (HPC) generously provided by the Technical Univer-

Figure 3.11: An illustrative depiction of an HPC cluster.

sity of Delft. This HPC environment delivers the computational potency and resources essential for conducting in-depth simulations, thereby ensuring the precision and reliability of our research outcomes.

Cluster Configuration

The HPC clusters employed in our research adopt the Beowulf style cluster architecture. Typically, a Beowulf-style cluster consists of a master node and several worker nodes. The master node serves as the hub where users log in, prepare, and manage parallel jobs. It houses both a scheduler (Maui) and a resource manager (Torque), operating synergistically to facilitate job submissions that are executed on the worker nodes, where the actual parallel processing occurs. These worker nodes are standalone computers interconnected via a local network to the master node and await instructions from the scheduler and resource manager to execute parallel jobs.

The HPC11 cluster, a prominent component of our research infrastructure, comprises a total of 45 nodes, collectively accommodating 1744 processing cores. This substantial computing power was instrumental in handling the computationally intensive three-dimensional (3D) simulations essential for our research. For each 3D simulation, we utilized a single node equipped with 24 CPUs, leveraging the OpenMP framework. Although larger scenarios often benefit from multiple nodes with communication and distribution facilitated through the MPI framework, our extensive testing revealed that, for this specific case, the optimal approach favored employing a single node utilizing the OpenMP methodology. The use of HPC was primarily driven by the computational demands imposed by our 3D simulations, which required substantial parallel processing capabilities for accurate and efficient modeling.

Chapter 4

Results and Analysis

4.1 Introduction

This section presents the findings of our qualitative investigation, organized into two segments. We begin by presenting the results from the two-dimensional cases, followed by the three-dimensional case. Our study involves a comprehensive comparative analysis of three distinct biochemical models. These models undergo a three-fold evaluation: an intra-scenario comparison, a congruence assessment with other computational study, and direct alignment with empirical data. This systematic approach comprehensively assesses the efficacy and relevance of our models.

Each biochemical model undergoes distinct calibration and generation processes, resulting in unique characteristics and weights. It's worth noting that the available data predominantly exhibit qualitative attributes, stemming from both experimental investigations and computational simulations.

The primary objective of this research is to ascertain the reliability of the viscosity increase model and its practical implications. The inherent patient-to-patient heterogeneity, affecting biochemical model parameters and geometrical factors, is a critical consideration.

The initial phase involves using the three biochemical models to generate unbiased results, enabling comparisons based on geometrical properties and temporal evolution. Subsequently, fully developed clot morphology is subjected to comparative analysis against computational studies and experimental data.

In the experiment conducted by [8], two distinct modes for whole blood perfusion were established: a constant flow rate mode and a pressure relief mode. The constant flow rate mode offers precise experimental control, but thrombotic occlusion cannot occur. In contrast, the pressure relief mode, more physiologically relevant, diverts flow away from channels undergoing thrombotic occlusion. For simplicity and numerical stability, this thesis implemented the constant flow rate mode.

4.2 Two-Dimensional Case

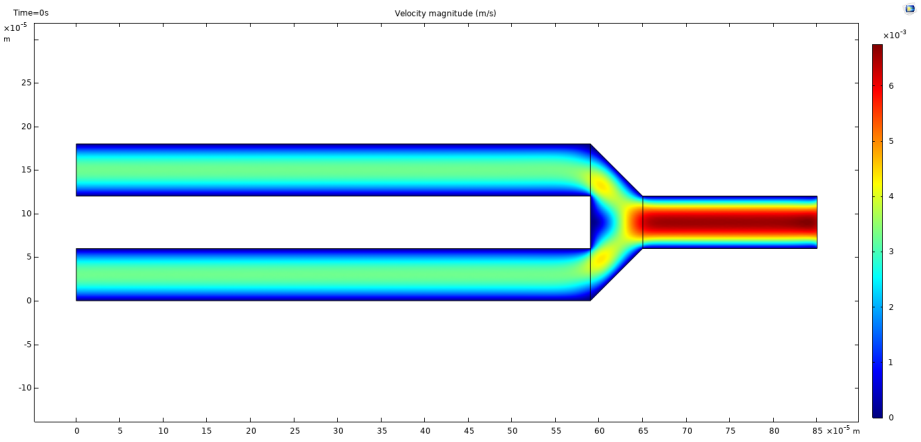

Figure 4.1: Initial Velocity Profile of the Two-Dimensional Geometry

In this section, we present the results obtained from the two-dimensional cases of our study, which are essential for understanding the behavior of the biochemical models in simplified scenarios. The primary aim is to replicate the fully developed clot scenario as reported in the literature.

It's important to note that most graphical representations have undergone a normalization process. This normalization ensures a rigorous and unambiguous comparative analysis among the various models under consideration.

The main focus of the generated plots is on the fully developed clot scenario at $t = 260$ seconds. However, supplementary plots, including additional time points, are provided in the appendix for a more comprehensive examination of the thrombotic process.

4.2.1 Concentration Propagation Comparison

In this context, three discrete locations were strategically identified along the axis bisecting the inflammation region within the channel. These locations represent specific distances, precisely 1%, 25%, and 50% of the total span from the inflammation region to the upper channel boundary.

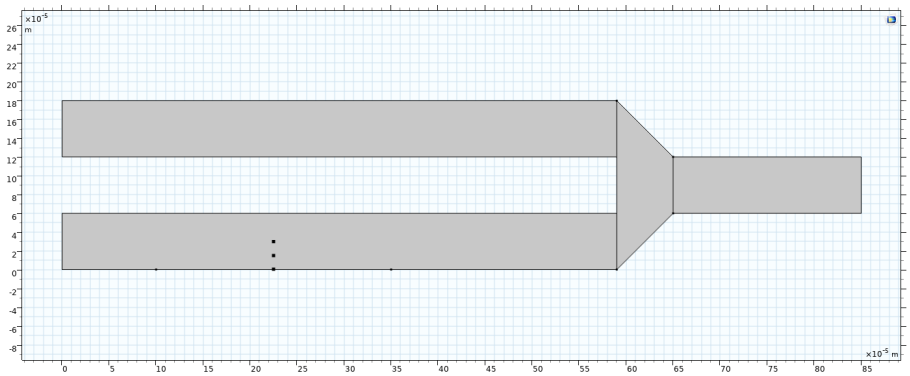

Figure 4.2: The three selected locations for comparisson.

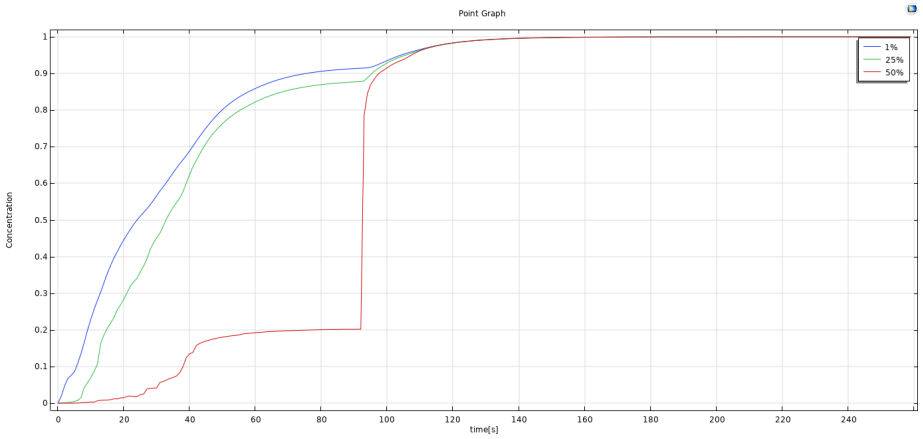

Figure 4.3: Bodnar 7-species model, 1%,25% and 50% fibrin concentration comparison.

In this section, discernible distinctions in the behavior of each biochemistry model come to light. The 7-species model exhibits a gradual concentration increase in the initial seconds, with the concentration at the 50% point reaching the critical clotting value , after which it exhibits a rapid ascent. These instantaneous viscosity variations pose numerical challenges, a characteristic also reflected in the computational time, with this model registering the slowest

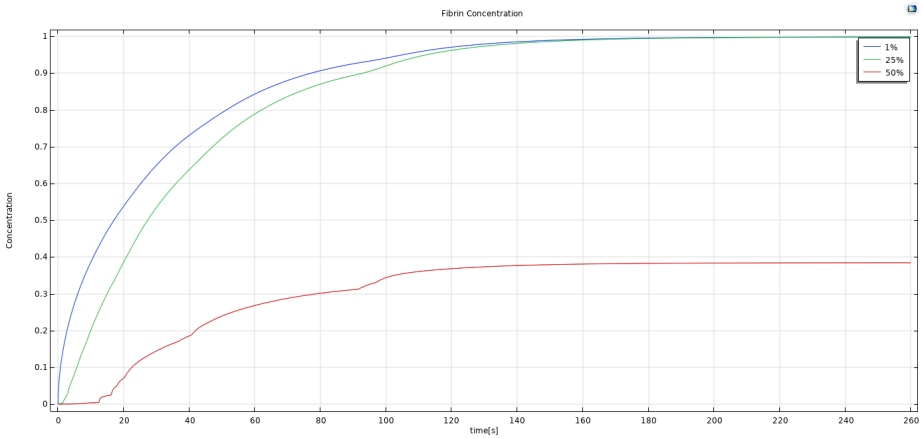

Figure 4.4: One-species model, 1%,25% and 50% fibrin concentration comparison.

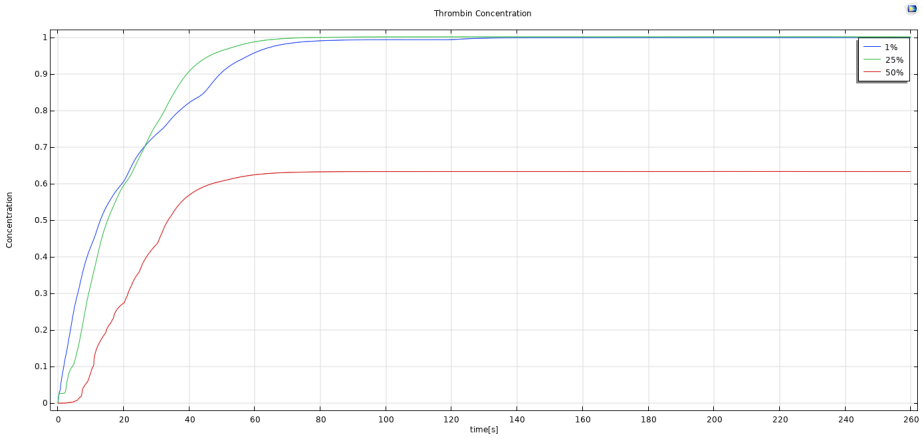

Figure 4.5: Papadopoulos 4-species model, 1%,25% and 50% fibrin concentration comparison.

performance.

4.2.2 Shear rate

Shear rate profiles can be seen in figure 4.6. When it comes to locating the areas for a possible build-up or decrease of the blood clot, it is necessary to find areas of low and high shear rate. As the viscosity depends highly on the shear rate, it means that at areas of low shear rate, viscosity is high and so the fibrin is going to build up in those areas.

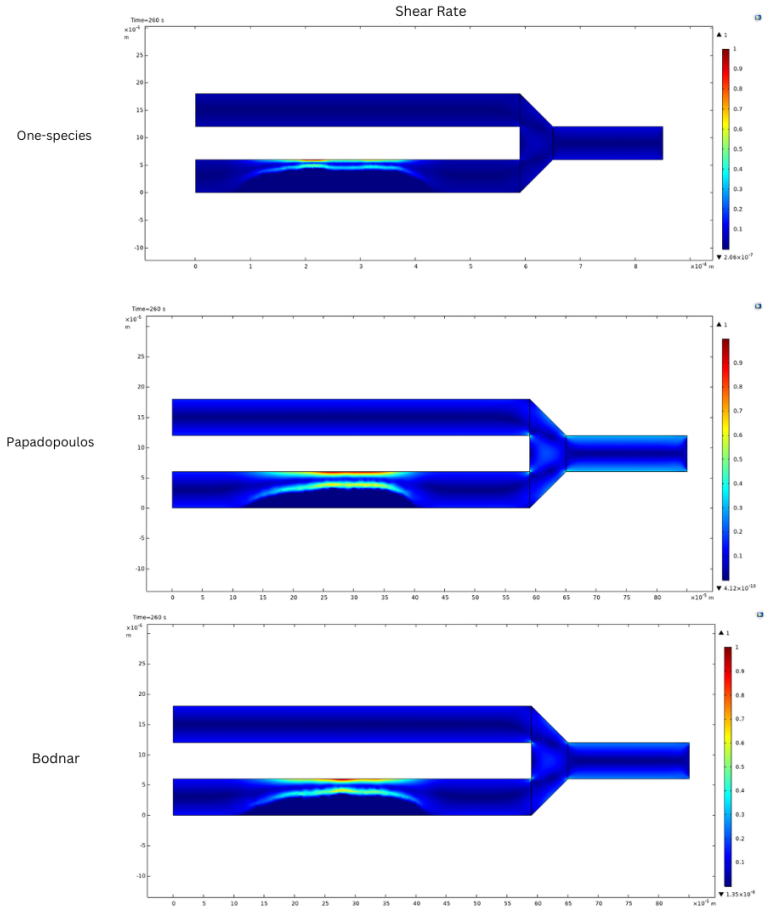

Figure 4.6: One-species, Papadopoulos and Bodnar models Shear rate surface plot for fully developed thrombus t=260s.

In our case we can observe the points in figure 4.6 on the formed clot with high shear rate that correlate to fibrin attachment. Also the highest shear rate regions are between the clot and the top channel boundary witch makes sense

since the highest values of velocity are there.

4.2.3 Velocity

The velocity profiles in Figure 4.7 serve as valuable tools for enhancing our comprehension of the clot's influence on blood flow dynamics. In our specific case, the outcomes align with our expectations, illustrating that the highest velocity values occur in the upper region of the clot. This phenomenon is observed to ensure the fulfillment of the conservation of mass.

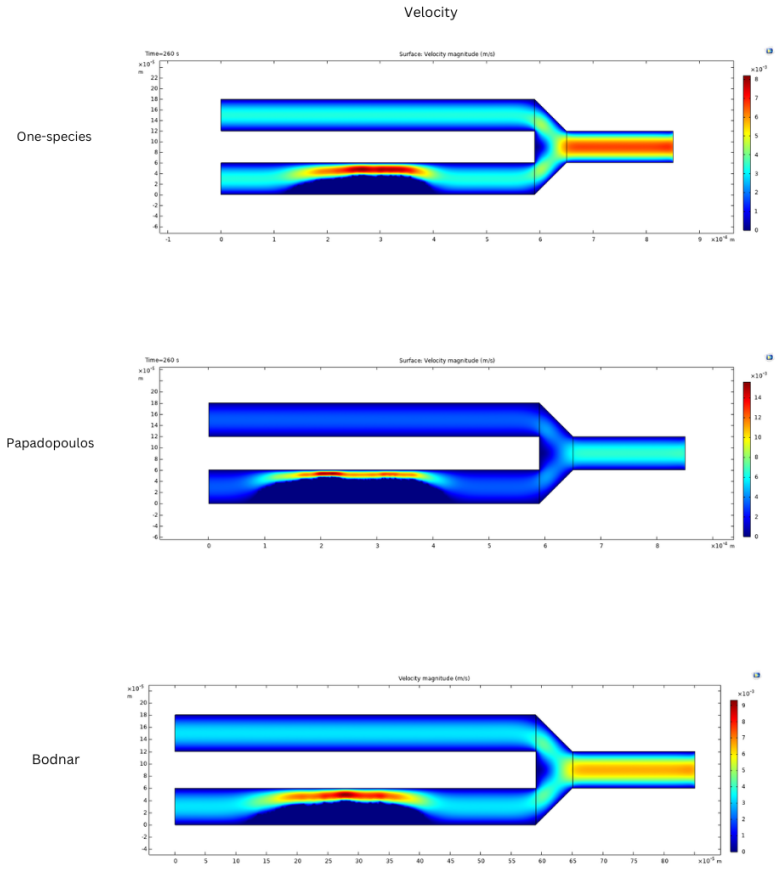

Figure 4.7: One-species, Papadopoulos and Bodnar models Velocity surface plots for fully developed thrombus t=260s.

4.2.4 Dynamic Viscosity

In this context, the dynamic viscosity plots in Figure 4.8 offer valuable insights into the actual region affected by clot formation. Among the models considered, the one-species model stands out as the most efficient, generating a substantial clotted area, which holds promise for specific scenarios. However, it has limitations since its manipulable parameter is solely the inflammation surface concentration or flux. On the other hand, both the Bodnar and Papadopoulos models consistently stabilize and yield reasonably comparable clotted regions.

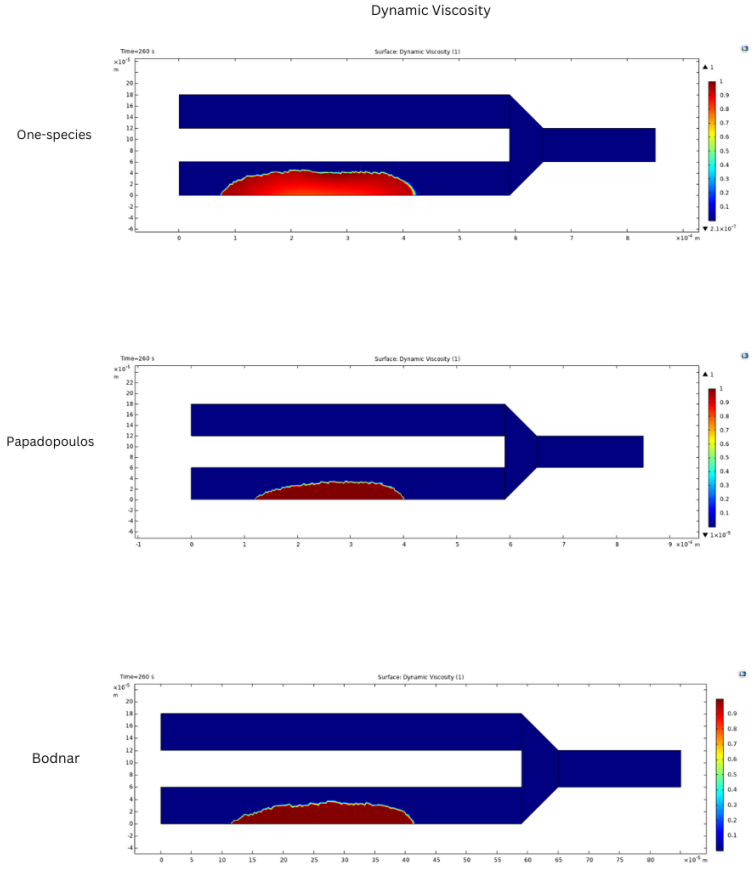

Figure 4.8: One-species, Papadopoulos and Bodnar models Dynamic Viscosity surface plots for fully developed thrombus t=260s.

4.2.5 Coagulant Concentration

The concentration plots in Figure 4.9 provide a comprehensive view of the distribution of key biochemical species within the clot formation region. Notably, the one-species model exhibits a distinct concentration profile, which correlates with its efficient clot formation characteristics. However, its applicability remains restricted to scenarios where the inflammation surface concentration or flux is the primary variable of interest. In contrast, the Bodnar and Papadopoulos models consistently produce concentration profiles that closely align with each other, demonstrating their reliability in capturing the clot formation process.

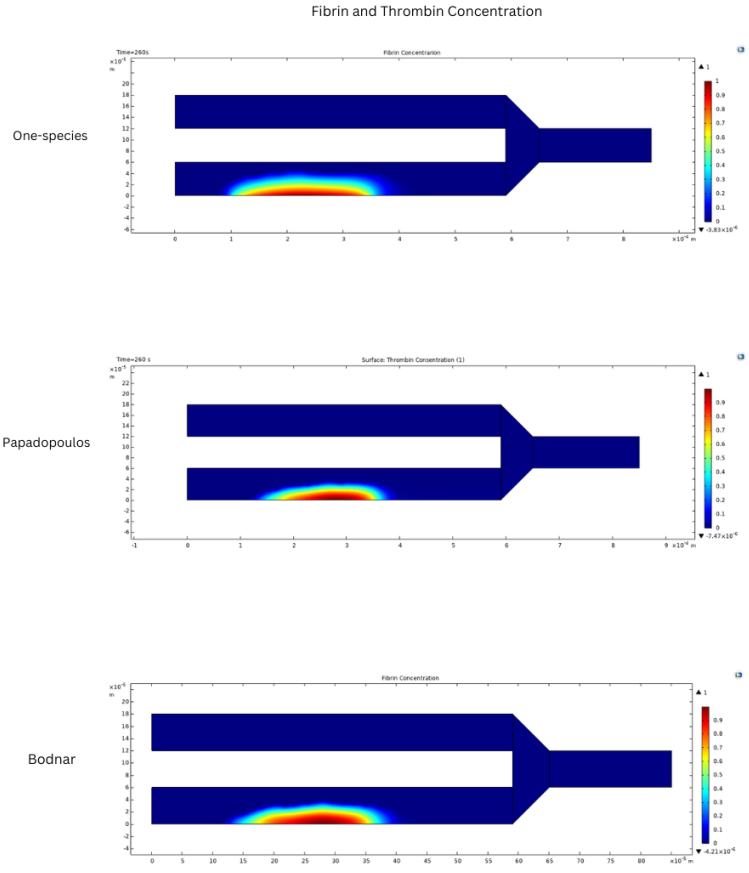

Figure 4.9: One-species, Papadopoulos and Bodnar models Fibrin and Thrombin concentration surface plots for fully developed thrombus t=260s.

4.2.6 Model Comparisons

The three models employed in this study, while useful in their own right, embody simplifications that limit their capacity to replicate real-life thrombosis dynamics accurately. Our primary focus was the rigorous validation of the 7-species model, which had shown promise in previous studies but lacked empirical validation. During this validation process, coupled with the Viscosity Variation Method, unexpected complexities emerged, emphasizing the need for a comprehensive understanding of the model's capabilities and limitations. While this model held significant potential, our research revealed unanticipated issues and discrepancies, underscoring the challenges in using simplified biochemical models for thrombosis simulation.

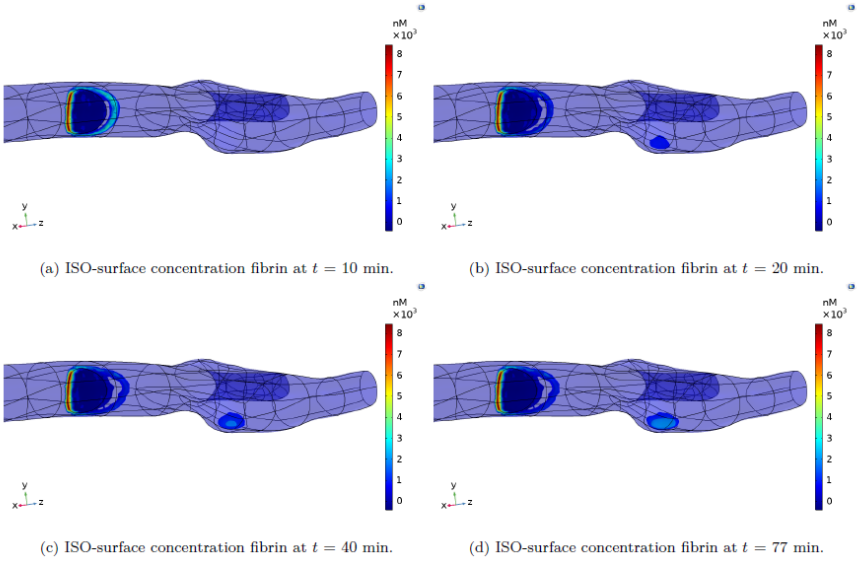

(a) ISO-surface concentration fibrin at $t = 10$ min.

(b) ISO-surface concentration fibrin at $t = 20$ min.

(c) ISO-surface concentration fibrin at $t = 40$ min.

(d) ISO-surface concentration fibrin at $t = 77$ min.

Figure 4.10: ISO-surface fibrin concentrations at different times. This study conducted by L.Corsini on a thrombosis simulation in a patient specific geometry of a Carotid Artery.

The models' capacity to attain the requisite concentration for phase change, as originally utilized by its creator Bodnar, was found to be insufficient due to the small dimensions and extremely low flow velocities associated with a low Reynolds number (Re=0.023). This unfavorable setting notably impacted the behavior of thrombotic species.

In light of the model's inadequacy in reproducing experimental data, two alternative validation methods were devised. These methods aimed not only to confirm the model's ineffectiveness but also to offer a more balanced approach for scenarios focused on spatial development, granting researchers greater control over problem parameters.

The one-species model was introduced as a control model, characterized by its uniformity and lack of intuitive control in tandem with fluid dynamics. Notably, this model resulted in the most substantial obstruction and posed challenges in configuring its surface Fibrin flux, denoted as $J_{cIa} = 5{\cdot}10^{-10}[mol/(m^2 \cdot s)]$.

The Papadopoulos Model is selected for the 3D simulation due to its balanced attributes of simplicity, sufficient spatial development, and configurability.

4.2.7 Comparison with Computational Studies

In our comparative analysis, we align our two-dimensional findings with a pertinent computational study conducted by Mohammad Rezaeimoghaddam and Frans N. van de Vosse [19]. Their research offers a comprehensive approach to modeling thrombus formation and growth. Notably, they developed an intricate biochemical model for platelet activation and aggregation, aiming to predict the size and shape of thrombi that manifest at sites of vascular injury. Employing computational fluid dynamics, specifically the finite volume method, they computed velocity and pressure fields influenced by evolving thrombi.

Their research encompassed solving a set of convection–diffusion–reaction equations, which account for the passive transport of platelets, agonists, platelet activation kinetics, platelet adhesion to growing thrombi, and platelet embolization. To initiate thrombus formation, they introduced a thrombogenic surface representing either blood-contacting material or injured blood vessels as a surface flux boundary condition. Their model treated blood as a Newtonian fluid while regarding the thrombus as a porous medium.

It's worth noting that their study, similar to ours [19], replicates the same case, albeit through a two-dimensional simulation.

In figure 4.19 the spatial and temporal development of thrombus formation within the thrombogenic channel is illustrated. The solid black lines represent experimental data obtained by Colace et al. (2012) [8], while the light orange volumes depict the calculated concentrations of deposited blood platelets. The vertical dashed lines indicate the length of the thrombogenic surface.

The two experiments share identical boundary conditions and rheological parameters, differing solely in the biochemical and clot formation models employed. Ignoring temporal development disparities, the Papadopoulos model yields a more uniform clot with a slightly higher downstream side, contrasting with the computational study's results, which exhibit the opposite behavior. This discrepancy can be attributed to the variations in the phase change model and platelet adhesion model between the two approaches. These distinct models promote different flow characteristics and exert significant influence on species diffusion dynamics.

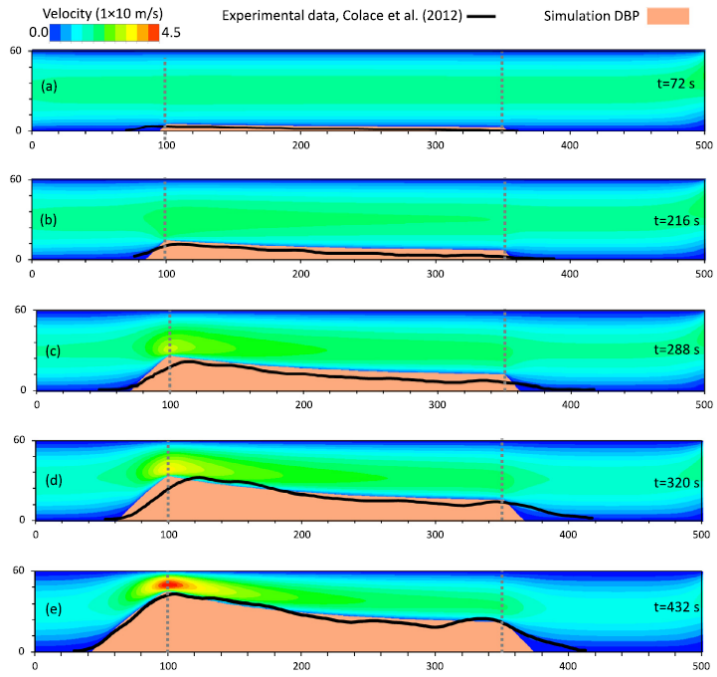

Figure 4.11: Figures (a) to (e) present phase visualizations of DBP, profiles of platelet deposition, and contours of velocity magnitude at times t = 72 s, 216 s, 288 s, 360 s, and 432 s, respectively.

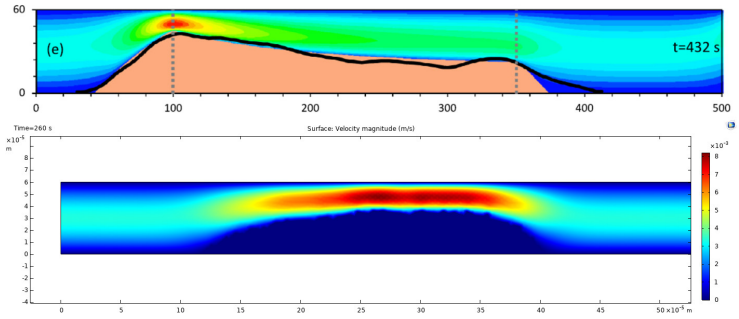

Figure 4.12: The top figure presents the fully developed Thrombus at t=432 seconds alongside the velocity profile obtained from the computational study. In the bottom figure, we observe the velocity profile of Papadopoulos's model for a fully developed clot at t=260 seconds.

4.3 Three-Dimensional Case

In this section, we shift our focus to the three-dimensional case, which offers a more complex and realistic representation of the coagulation process. Only results for the Papadopoulos model are presented here.

4.3.1 Velocity, Shear Rate, Dynamic Viscosity and Concentration

Beginning with the examination of the 3D velocity plots, it becomes evident that the outcomes differ significantly from those observed in the 2D scenario. Firstly, the formation of the clot predominantly occurs on the channel's lateral sides. This observation aligns with physical expectations, as a larger horizontal dimension implies that pressure is more likely to accumulate vertically and disperse horizontally.

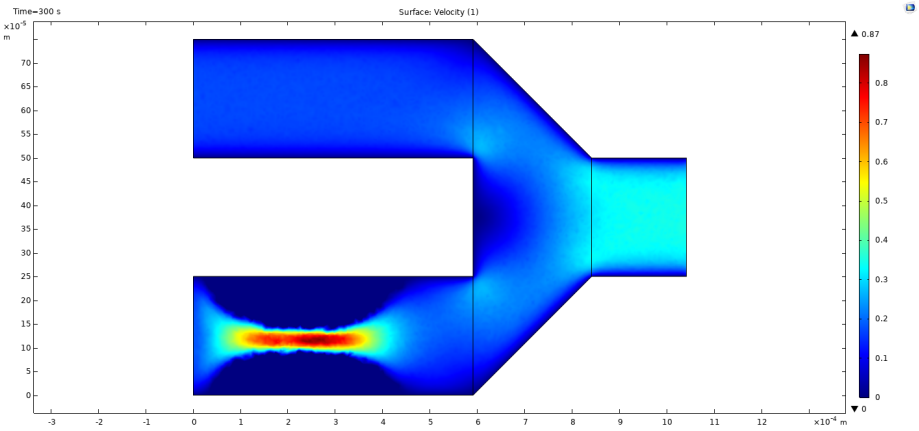

Figure 4.13: Velocity Contour at 20μm height.

In the bird's-eye view depicted in Figures 4.21 4.22 4.23, it's noticeable that the vertical development in the center of the channel, starting from 2/6 of the height in Figure 1 and descending to 1/60 of the height, exists but remains relatively insignificant.

In this depiction, we observe the complete course of blood flow and the degree of obstruction it encounters.

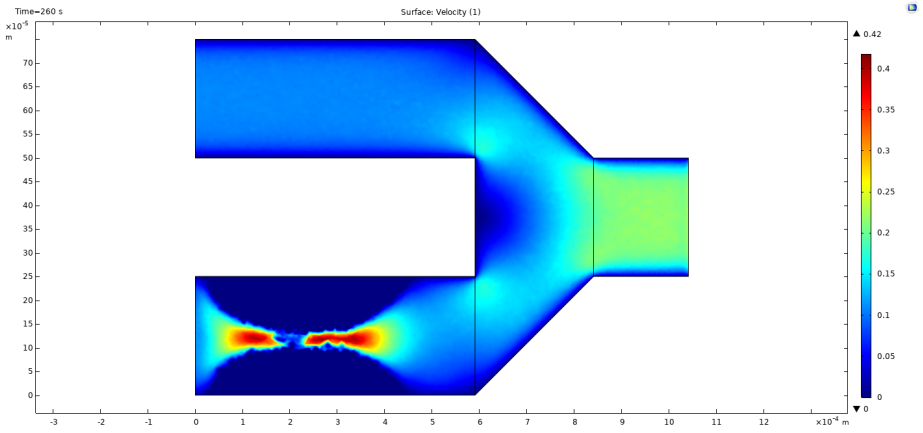

Figure 4.14: Velocity Contour at 10μm height.

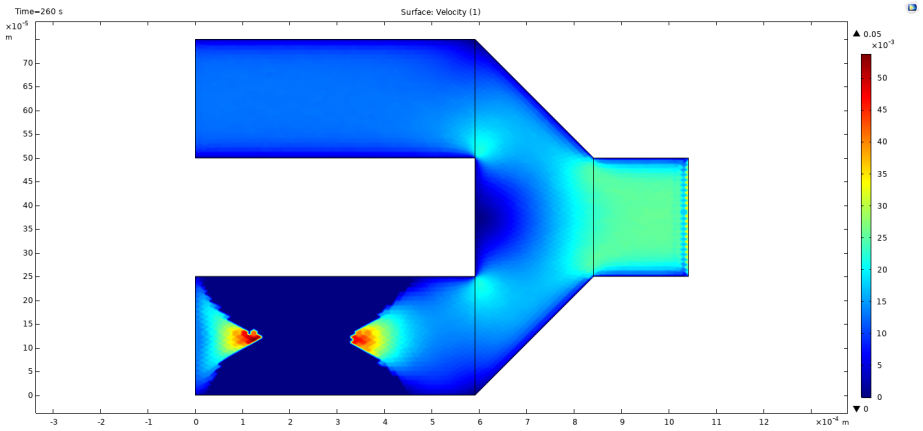

Figure 4.15: Velocity Contour at 1μm height.

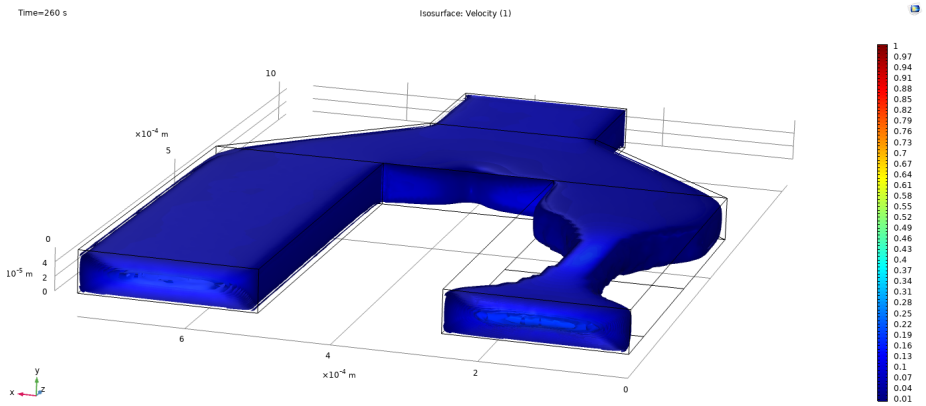

Figure 4.16: Velocity ISO-surface. (t=260s)

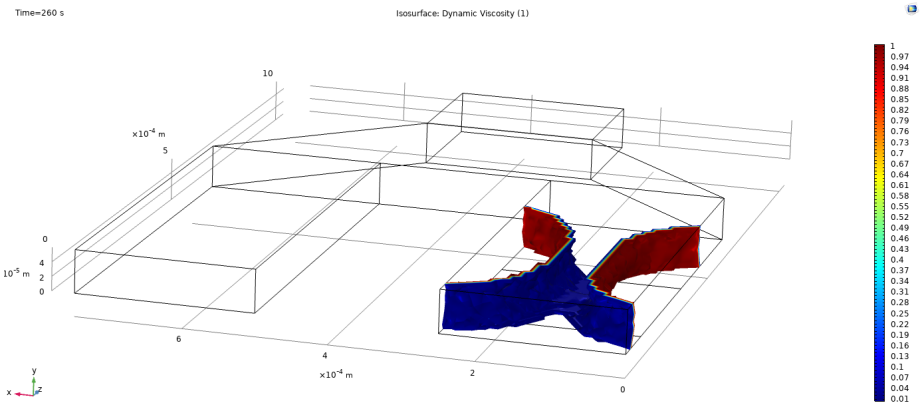

Figure 4.17: Dynamic Viscosity ISO-surface defining the thrombus shell formed. (t=260s)

In the viscosity and concentration plots, the geometry of the thrombotic region becomes evidently clear. The development of increased viscosity cells is seen propagating from various angles, effectively transforming the channel flow into a nearly pipe-like configuration for a segment of the clot's length.

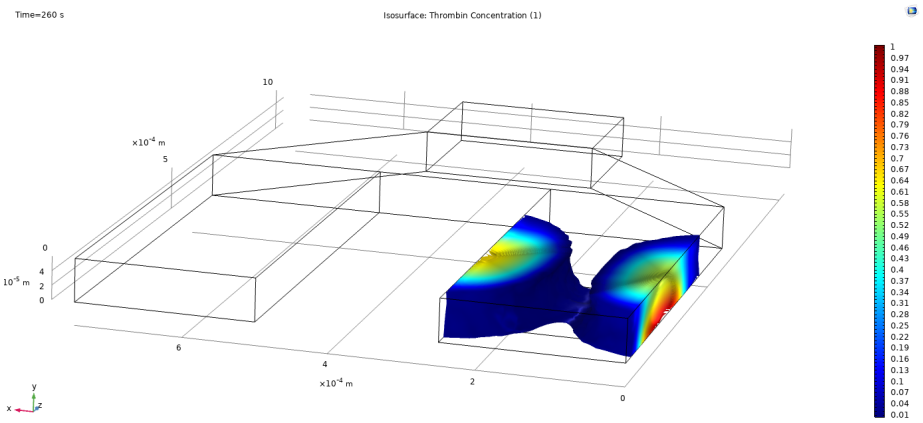

Figure 4.18: Thrombin Consentration ISO-surface. (t=260s)

Chapter 5

Discussion

5.1 Interpretation of Results

While the two-dimensional scenario aligns with existing spatial concepts in the literature, the three-dimensional depiction takes a distinct form, primarily due to the dominant influence of shear stress on clot morphology.

The transition from a liquid to a solid state occurs gradually, guided by factors like fibrin or thrombin production in accordance with the biochemical model and boundary conditions. Once this transition is complete and the thrombus stabilizes, viscosity immediately and significantly increases, primarily due to diffusion being the sole transport mechanism. The solid phase region, however, tends to underestimate the complexity of reactions and interactions, suggesting potential applicability of a porous material model.

This geometry essentially adheres to the vessel wall without displaying detachment or shape alteration under the influence of flow. While the current analyses provide valuable insights, more extensive investigations are warranted for geometries at elevated Reynolds numbers that mimic real-world conditions. The Viscosity Variation model, despite its simplicity and suitability for flow characterization-focused work, has not yet been validated against experimental data.

In my assessment, the model falls short in accurately reproducing real-world data, particularly in terms of clot morphology. To enhance its representational capacity, one could explore the possibility of integrating Papadopoulos' biochemical model with optimization techniques for spatially replicating experimental data. This approach holds promise for achieving a more precise calibration of system parameters, aligning computational outcomes with real-world observations.

5.2 Strengths and Limitations

In my diligent pursuit of model validation through the utilization of three distinct biochemical models, several enlightening conclusions have emerged. Notably, the model exhibits a pronounced trait of computational efficiency, rendering it exceptionally user-friendly. This intrinsic lightness in computational demand facilitates ease of use, making it accessible to researchers across various domains.

Remarkably, the model's robustness shines through even when employed on sparser grids. This remarkable quality enables a crude yet insightful personification of the effects of thrombosis on the rheological characteristics within stenotic scenarios.

Furthermore, the model's simplicity proves to be a pivotal advantage, as it seamlessly integrates with diverse research endeavors. Its versatility extends beyond thrombosis simulations, offering opportunities for synergistic studies involving the circulatory system and related phenomena.

Moreover, the calibration process applied to Papadopoulos' model holds paramount significance. This feature empowers researchers to tailor the model to accommodate patient-specific parameters, a capability that is invaluable in personalized medicine and in-depth clinical investigations. This adaptability ensures that the model can be employed as a potent tool in addressing the unique intricacies of individual patients' conditions.

In sum, the strengths of this model are distinctly marked by its computational efficiency, adaptability, and synergy with a range of research domains. These attributes collectively enrich the researcher's toolkit, fostering deeper insights into thrombosis and related phenomena. However, it is essential to acknowledge the accompanying limitations, which underscore the necessity for ongoing refinement and validation to enhance the model's accuracy and clinical relevance.

5.3 Implications and Applications

The simplified 4-species coagulation model, rooted in the work of Papadopoulos, offers a concise and adequate spatial representation of thrombin generation dynamics. This model, with its emphasis on simplicity, carries several key implications and prospective applications:

1. **Efficient Simulations:** The model's simplicity ensures quicker computational runs, making it ideal for scenarios requiring multiple simulations or real-time analyses without compromising on key aspects of coagulation dynamics.

2. **Accessible Interpretation:** Due to its streamlined nature, the model can be more easily understood, making it suitable for educational purposes and for practitioners not specialized in computational modeling.

3. **Basis for Personalized Medicine:** With patient-specific calibrations, the model has the potential to inform tailored therapeutic strategies, aligning interventions with individual thrombin generation patterns.

4. **Research Tool:** In both academic and pharmaceutical contexts, the model can support studies focusing on the basics of thrombin generation, particularly when intricate species behaviors are not the primary concern.

5. **Integration into Larger Systems:** The model's simplicity makes it more amenable to integration within broader physiological models, enabling more holistic studies without the computational burden of more complex models.

The streamlined nature of this model, combining efficiency with a degree of accuracy, presents a valuable tool for diverse applications in the realm of coagulation studies.

5.4 Future Research

The research conducted in this study has shed light on various aspects of thrombosis modeling and its interaction with blood flow dynamics. However, several avenues for future research and exploration remain open, offering opportunities to enhance our understanding of this complex phenomenon.

An imprecision within the thrombosis model relates to the utilization of a step-function to induce an increase in viscosity. This approach was employed to mimic a solid blood clot capable of partially obstructing flow. However, the abrupt elevation in viscosity at a specific fibrin concentration threshold lacks a rigorous basis. An alternative approach could involve simulating thrombus formation in two phases: the initial phase modeling thrombosis within the first few minutes without an additional viscosity increase, and the subsequent phase employing a solid object with identical geometry and physical properties as generated in the first phase. This approach could facilitate the simulation of emboli that can be carried by arterial flow, addressing a limitation of the current model where the clot merely stretches without detachment. Alternatively, adjusting the values of parameters b and c_{crit} could also yield a potential solution.

Throughout the utilization of COMSOL software in this thesis, various beneficial packages of physics modules and data acquisition functions were encountered, although most remained unused in this particular research endeavor. For future studies employing COMSOL, it is strongly recommended to gain a comprehensive understanding of the software's capabilities, encompassing its array of physics modules, functions, and measurement techniques, prior to initiating simulations. Of paramount importance is the necessity for user-controlled meshing, allowing for the creation of dynamic meshes or finer grids in regions with elevated fibrin concentrations, which would significantly enhance result accuracy.

5.5 Conclusion

Thrombosis, characterized by its intricate balance of cellular, biochemical, and hemodynamic elements, remains a prominent challenge to global health, contributing to significant morbidity and mortality. The multi-faceted nature of the condition mandates a comprehensive investigative approach to shed light on the nuanced mechanisms underpinning clot formation.

In this thesis, we embarked on a computational journey to demystify the dynamics of thrombosis. The developed model, grounded in principles from fluid dynamics, biochemistry, and reaction kinetics, brought forth a unique perspective by emphasizing fibrin or thrombin induced viscosity variation, an element that adds a novel dimension to thrombosis research. Utilizing COMSOL Multiphysics as the simulation platform provided an avenue to fuse the Navier-Stokes equations seamlessly with the biochemistry of coagulation, offering an integrative perspective on thrombosis.

Despite its theoretical robustness, our model encountered challenges during the validation phase against empirical data. This underscores the intricacies inherent in simulating biological phenomena and serves as a poignant reminder of the iterative nature of scientific endeavors. Yet, it's crucial to note that while the model may have its limitations in capturing intricate species behavior, its strength lies in portraying the spatial development of the clot. For research problems less concerned with the nuanced species behavior and more focused on the overall clot progression, our model offers a valuable tool.

This research, though preliminary in its findings, has nonetheless charted a path in thrombosis study. It serves as a foundational pillar upon which subsequent investigations can refine and build, both conceptually and computationally. Future endeavors might focus on honing the model, ensuring its predictive accuracy, and facilitating successful validation.

Our work underscores the pivotal role of computational modeling in advancing our comprehension of complex biological phenomena. Despite the encountered challenges, the research carries the promise of informing therapeutic strategies, particularly as the scientific community moves toward personalized interventions tailored for thrombotic disorders.

In summation, this thesis stands as a testament to the iterative journey of scientific discovery, highlighting the resilience required in the face of challenges and the unwavering pursuit of knowledge. The experiences documented here not only contribute to the ongoing discourse on thrombosis but also echo the broader sentiments of scientific rigor, adaptability, and innovation.

Bibliography

[1] Detailed explanation of the finite element method (fem). https://www.comsol.com/multiphysics/finite-element-method?parent= physics-pdes-numerical-042-62, february 2017.

[2] MUMPS: A parallel sparse direct solver. https://graal.ens-lyon.fr/MUMPS/index.php, July 2022.

[3] What are the navier-stokes equations, Sep 2023.

[4] L.R. Adams and I. Fatt. The diffusion coefficient of human hemoglobin at high concentrations. *Respiration Physiology*, 2(3):293–301, 1967.

[5] R. Byron Bird, Robert C. Armstrong, and Ole Hassager. *Dynamics of polymeric liquids, Volume 1: Fluid mechanics*. 2 edition, 1987.

[6] The Editors of Encyclopaedia Britannica. blood vessel. *Encyclopedia Britannica*, 2023.

[7] Cleveland Clinic. Thrombosis, 2021.

[8] Thomas V Colace, Ryan W Muthard, and Scott L Diamond. Thrombus growth and embolism on tissue factor-bearing collagen surfaces under flow: role of thrombin with and without fibrin. *Arterioscler Thromb Vasc Biol*, 32(6):1466–1476, apr 2012.

[9] B S Hertzberg, M A Kliewer, D M DeLong, K J Lalouche, E K Paulson, M G Frederick, and B A Carroll. Sonographic assessment of lower limb vein diameters: implications for the diagnosis and characterization of deep venous thrombosis. *American Journal of Roentgenology*, 168(5):1253–1257, 1997. PMID: 9129422.

[10] Jonghwun Jung and Ahmed Hassanein. Three-phase cfd analytical modeling of blood flow. *Medical Engineering Physics*, 30(1):91–103, 2008.

[11] Ye Li and Ashraf W. Khir. Experimental validation of non-invasive and fluid density independent methods for the determination of local wave speed and arrival time of reflected wave. *Journal of Biomechanics*, 44(7):1393–1399, 2011.

[12] S F Maloney, Lawrence F Brass, and S L Diamond. P2Y12 or P2Y1 inhibitors reduce platelet deposition in a microfluidic model of thrombosis while apyrase lacks efficacy under flow conditions. *Integr Biol (Camb)*, 2(4):183–192, January 2010.

[13] E. Marieb and K. Hoehn. *Human Anatomy & Physiology*. Pearson, 2016.

[14] E Marieb and K Hoehn. *Human anatomy & physiology/Elaine N. Marieb RN*. PhD thesis, Ph. D., Holyoke Community College, Katja Hoehn, MD, Ph. D, Mount Royal . . . , 2016.

[15] E.N. Marieb, K. Hoehn, and Pearson. *Human Anatomy and Physiology, Global Edition*. Always learning. Pearson Education, Limited, 2015.

[16] I.E. Mulder. Bsc thesis; developing a simplified model of deep vein thrombosis with pulsatile blood flow and different geometries. *TU Delft*, 2022.

[17] Konstantinos Papadopoulos. Flow effect on thrombus formation in stenosed coronary arteries: a computational study. Unpublished, 2015.

[18] Konstantinos P. Papadopoulos, Manolis Gavaises, and Chris Atkin. A simplified mathematical model for thrombin generation. *Medical Engineering Physics*, 36(2):196–204, 2014.

[19] Mohammad Rezaeimoghaddam and Frans N. van de Vosse. Continuum modeling of thrombus formation and growth under different shear rates. *Journal of Biomechanics*, 132:110915, 2022.

[20] Sarah Robertson and Mark Miller. Ambient air pollution and thrombosis. *Particle and Fibre Toxicology*, 15, 01 2018.

[21] Adélia Sequeira, Rafael F. Santos, and Tomáš Bodnár. Blood coagulation dynamics: mathematical modeling and stability results. *Mathematical Biosciences and Engineering*, 8(2):425–443, 2011.

[22] J. Thomas. Bsc thesis; development of a simplified model of deep vein thrombosis. *TU Delft*, 2022.

[23] Wikipedia contributors. Volumetric flow rate — Wikipedia, the free encyclopedia, 2023. [Online; accessed 6-June-2023].

[24] J. Wojnarowski. Numerical study of bileaf heart valves performance. In *International Scientific Practical Conference: Efficiency of Engineering Education in XX Century*, Donetsk, Ukraine, 2001.

Appendix A

Appendix

A.1 Papadopoulos Results

A.1.1 Two-Dimensional Contours for different time intances

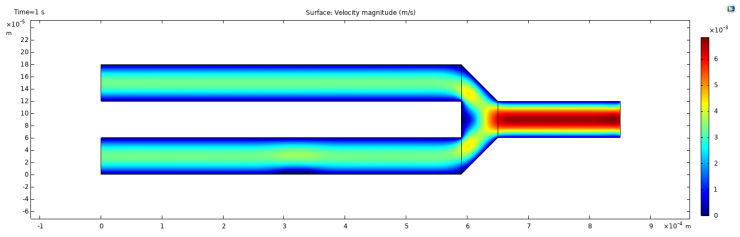

Figure A.1: vel t=1

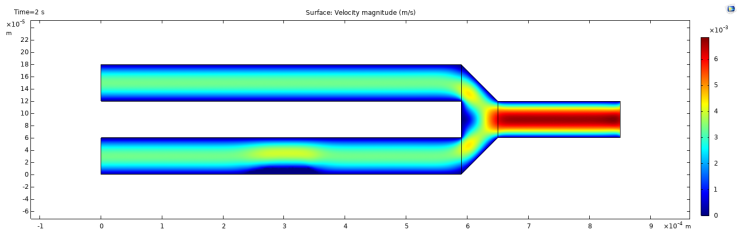

Figure A.2: vel t=2

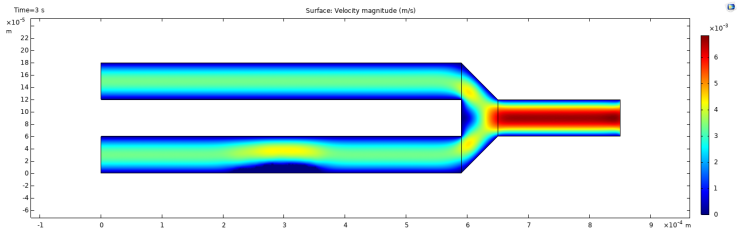

Figure A.3: vel t=3

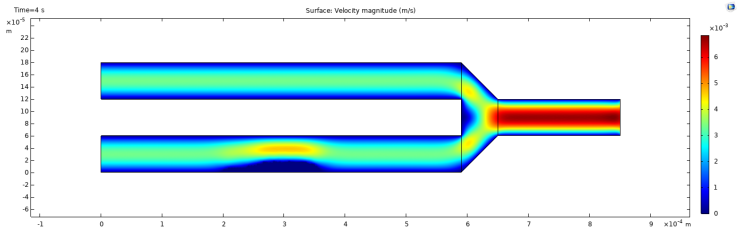

Figure A.4: vel t=4

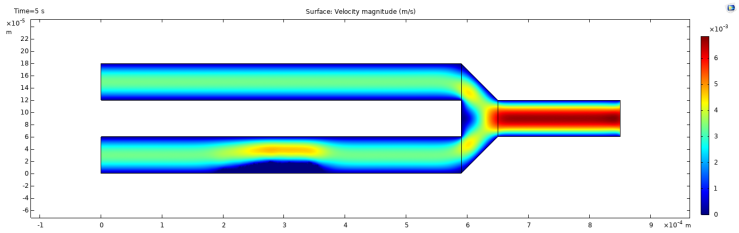

Figure A.5: vel t=5

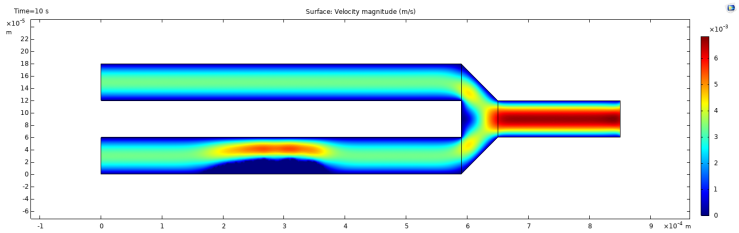

Figure A.6: vel t=10

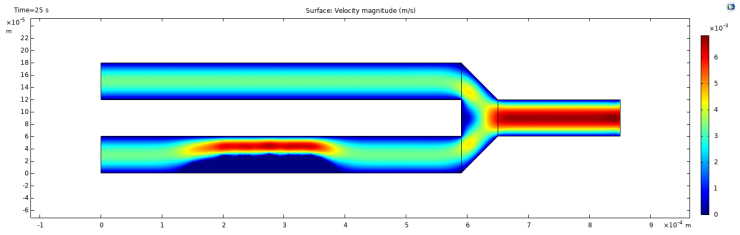

Figure A.7: vel t=25

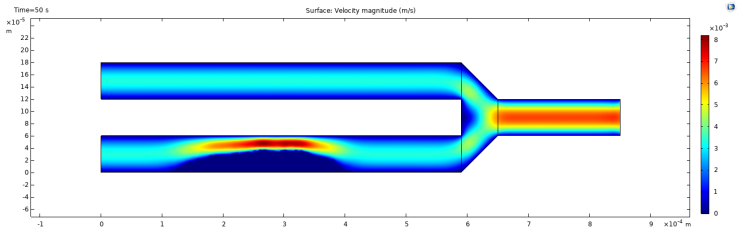

Figure A.8: vel t=50

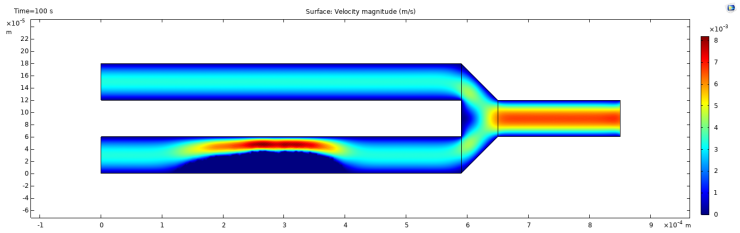

Figure A.9: vel t=100

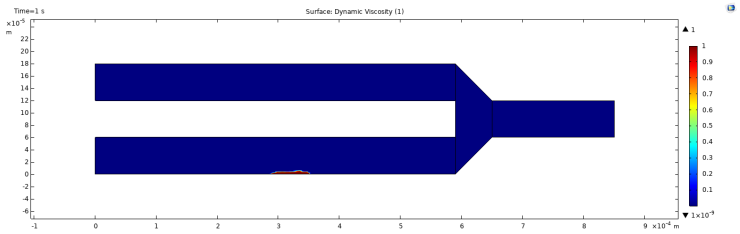

Figure A.10: Dynamic Viscosity t=1

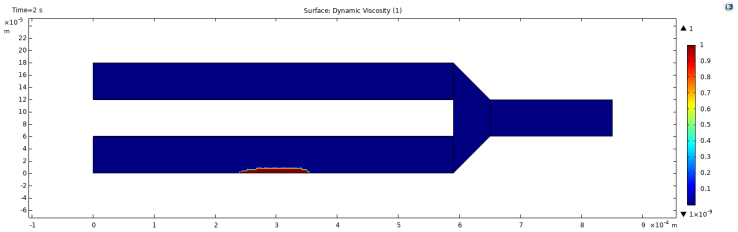

Figure A.11: Dynamic Viscosity t=2

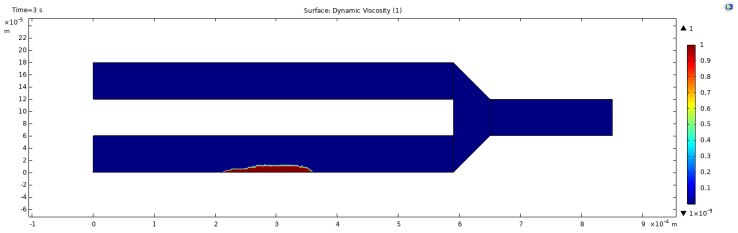

Figure A.12: Dynamic Viscosity t=3

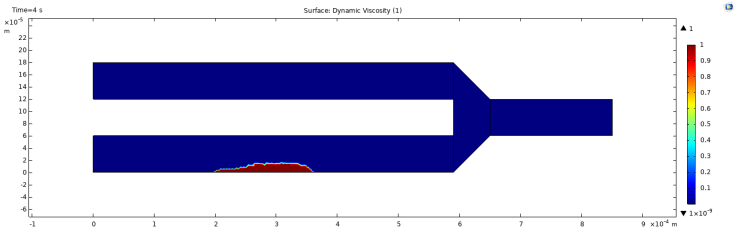

Figure A.13: Dynamic Viscosity t=4

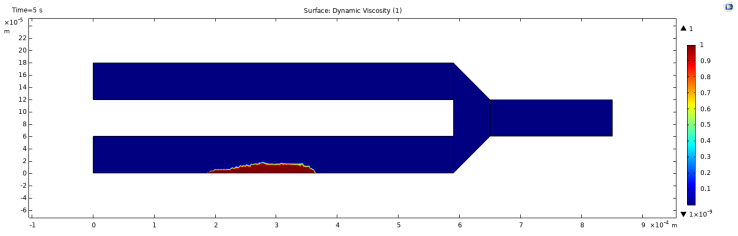

Figure A.14: Dynamic Viscosity t=5

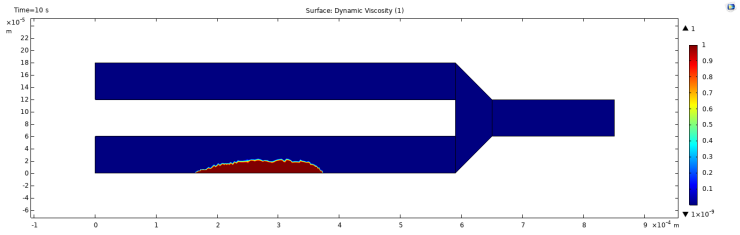

Figure A.15: Dynamic Viscosity t=10

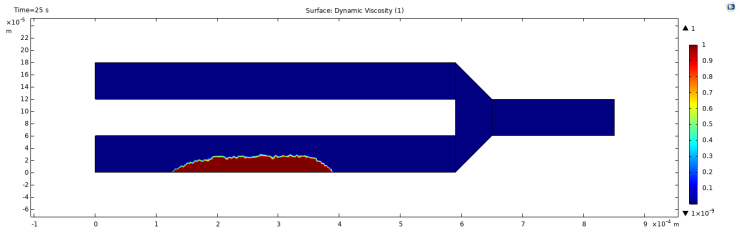

Figure A.16: Dynamic Viscosity t=25

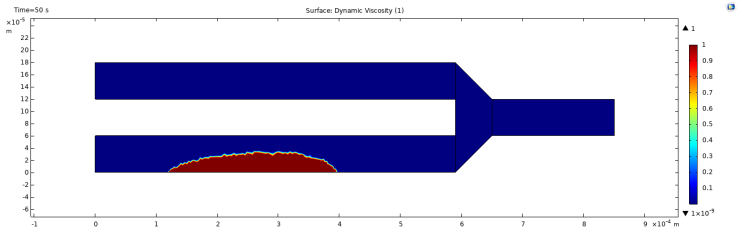

Figure A.17: Dynamic Viscosity t=50

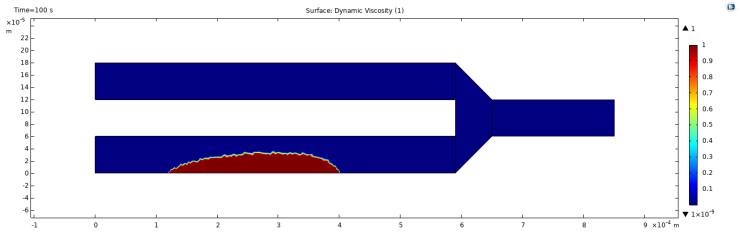

Figure A.18: Dynamic Viscosity t=100

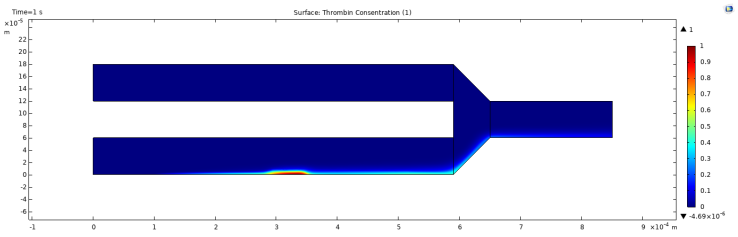

Figure A.19: Thrombin Concentration t=1

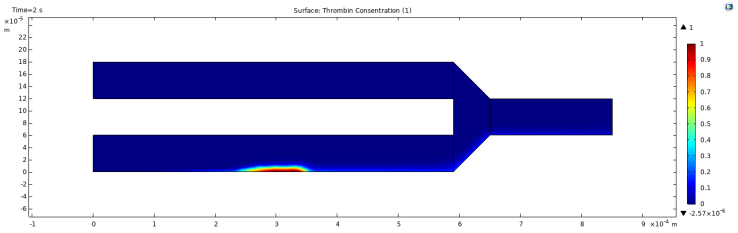

Figure A.20: Thrombin Concentration t=2

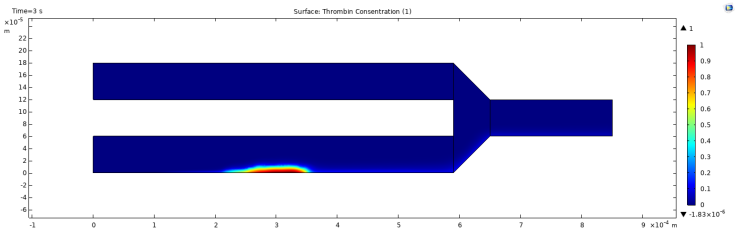

Figure A.21: Thrombin Concentration t=3

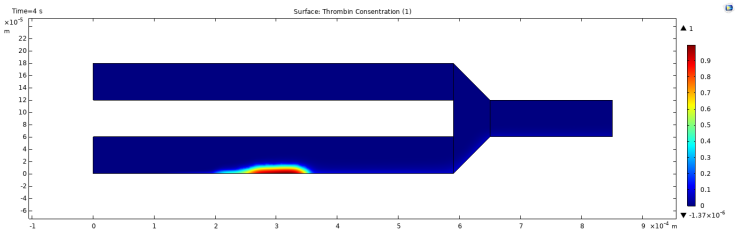

Figure A.22: Thrombin Concentration t=4

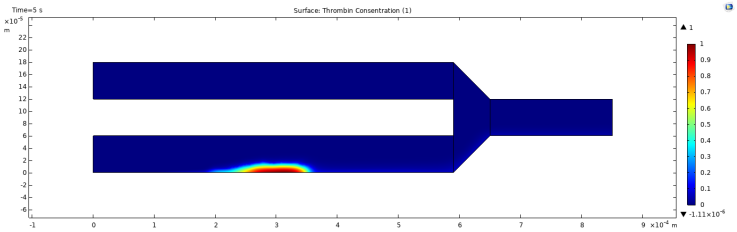

Figure A.23: Thrombin Concentration t=5

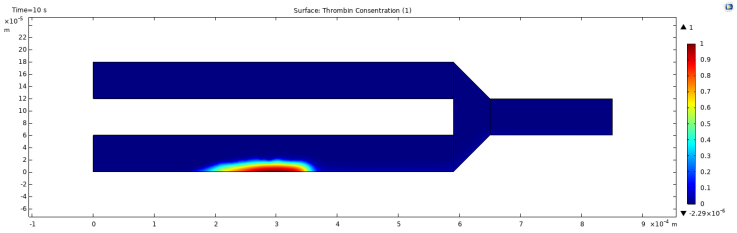

Figure A.24: Thrombin Concentration t=10

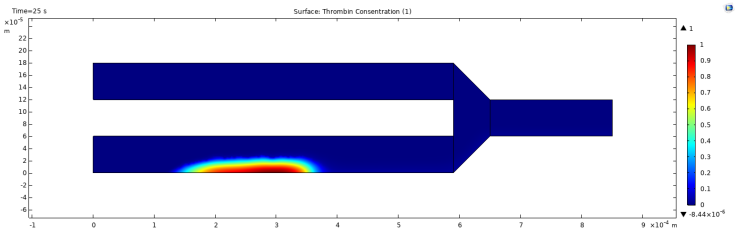

Figure A.25: Thrombin Concentration t=25

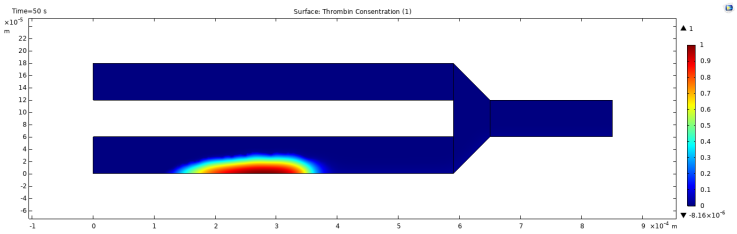

Figure A.26: Thrombin Concentration t=50

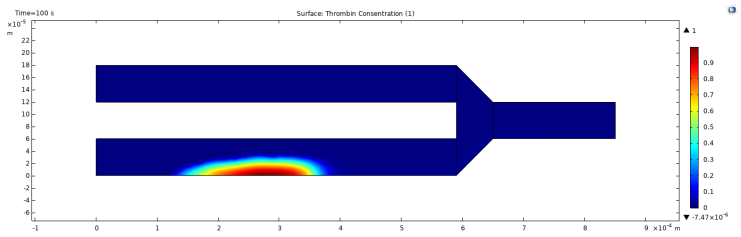

Figure A.27: Thrombin Concentration t=100